Non-Fermi-liquid states and pairing instability of a general model of copper oxide metals

C. M. Varma
Bell Laboratories, Lucent Technologies, Murray Hill, New Jersey 07974
(Received 17 July 1996)

A model of copper-oxygen bonding and antibonding bands with the most general two-body interactions allowable by symmetry is considered. The model has a continuous transition as a function of hole density x and temperature T to a phase in which a current circulates in each unit cell. This phase preserves the translational symmetry of the lattice while breaking time-reversal invariance and fourfold rotational symmetry. The product of time reversal and fourfold rotation is preserved. The circulating current phase terminates at a critical point at $x=x_c$, $T=0$. In the quantum critical region about this point the logarithm of the frequency of the current fluctuations scales with their momentum. The microscopic basis for the marginal Fermi-liquid phenemenology and the observed long-wavelength transport anomalies near $x=x_c$ are derived from such fluctuations. The symmetry of the current fluctuations is such that the associated magnetic field fluctuations are absent at oxygen sites and have the correct form to explain the anomalous copper nuclear relaxation rate. Crossovers to the Fermi-liquid phase on either side of x_c and the role of disorder are briefly considered. The current fluctuations promote superconductive instability with a propensity towards ''D-wave'' symmetry or ''extended S-wave''symmetry depending on details of the band structure. Several experiments are proposed to test the theory. [S0163-1829(97)09121-2]

I. INTRODUCTION

Besides their exceptionally high superconducting transition temperatures, copper-oxide- (Cu-O-) based metals also have exceptional normal-state properties.[1] Landau Fermi-liquid theory[2] and associated quasiparticle concepts, which are a foundation stone for much of our understanding of phenomena in condensed matter, appear to be inapplicable to their normal state. The principal problem is the development of a *consistent* theoretical framework in which the unusual metallic properties can be understood. Moreover, it is *necessary* to have a theory for the normal state to understand the mechanism of the superconductive instability.

Every transport property in the normal state of copper-oxide metals has a temperature dependence unlike other metals. For example, the electrical resistivity has a linear temperature dependence down to T_c for composition near the highest T_c for any class of Cu-O compounds even when that T_c is as low as 10 K.[3] On the other hand, the equilibrium properties, such as specific heat C_v and magnetic susceptibility χ are consistent with the usual temperature dependence and are in fact only about a factor of 2 enhanced over band-structure calculations.[4] The copper-oxide metals are thus qualitatively different from liquid ^{3}He and heavy fermion metals where strong interactions produce strong quantitative renormalizations in both equilibrium and transport properties without changing the asymptotic low-temperature dependences and which are properly called Fermi liquids.

Recent reexaminations[5] of the foundations of Landau's Fermi-liquid theory have confirmed the robustness of the theory for dimensions higher than 1 for any Hamiltonian with nonsingular low-energy interactions.[6] Therefore a principal part of the theoretical task is to show that, in a model appropriate for copper-oxide metals, elimination of the high-energy degrees of freedom leads to a singular effective low-energy Hamiltonian. The tremendous variety and number of experiments on copper-oxide metals severely constrain the form of such a low-energy Hamiltonian.

A. Constraints from experiments

A schematic generic phase diagram is drawn in Fig. 1 on the basis of the resistivity data. Where measurements are available every other transport property shows corresponding regions. The insulating-antiferromagnetic phase near 1/2 filling and the superconducting phase are shown in bold lines. The normal state is roughly divided into four regions with dashed lines representing crossovers from one characteristic temperature dependence in transport properties to another.

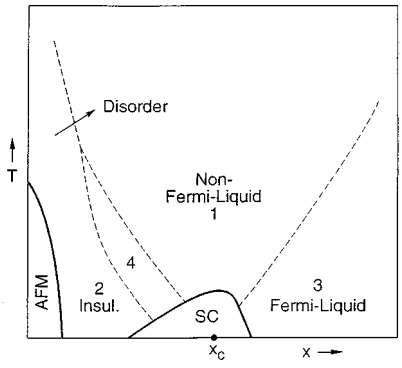

FIG. 1. Schematic generic phase diagram of the quasi-two-dimensional copper-oxide compounds. x is the density of holes doped in the planes. x_c is the ''optimum'' composition. The antiferromagnetic phase and the superconducting phases, shown inside solid lines, occur through phase transitions. A series of crossovers shown through dashed lines are discussed in the text. The impurity density, as inferred from the extrapolation of the high-temperature resistivity to $T=0$, i.e. assuming Mattheisen's rule, decreases as x increases. The size of region 4 decreases with increasing disorder for a given x.

Region 1, the non-Fermi-liquid phase, has $\rho(T)\approx\rho_0+\rho_1 T$ and similarly remarkable ''simple'' anomalies in all the other transport properties. In Bi 2201 resistivity measurements[3] are available from 10 to 800 K and in $La_{1.85}Sr_{0.15}CuO_4$ from 40 to 800 K.[7] The measured resistivity exponent in both is 1.05 ± 0.05. We may safely assume that it is 1 with possible logarithmic corrections. Such a behavior is observed only in a very narrow region near x_c. $\rho(T)$ begins to *decrease* below the linear extrapolation as temperature is decreased in region 3 and is consistent with an asymptotic T^2 dependence characteristic of a Fermi liquid. On the low doping side, in region 2, there is a crossover to resistivity increasing with decreasing temperature. This regime may be termed insulating. Strictly speaking, one should draw a third axis in Fig. 1 labeled disorder. If the zero-temperature intercept of the high-temperature linear-resistivity is taken as a measure of disorder, one concludes that it generally increases in the available data as x decreases. The limited systematic data with independent variation of disorder and x clearly shows that impurities have a dramatic effect in the underdoped regime while in the overdoped regime, region 3, their effect is conventional.[9]

The size of region 4 between region 1 and region 2 on the underdoped side depends upon disorder. The crossover between region 1 and region 4 is marked by a decrease in C_v/T and χ with temperature with their ratio almost independent of temperature.[4] In region 4 the resistivity drops below the linear extrapolation from region 1. This region has been termed the spin-gap region, but this is a misnomer. Not only do magnetic fluctuations, but optical conductivity and Raman scattering intensity in all measured polarizations decrease at low energies from their value in region 1. In region 2 this decline continues while the resisitivity begins to increase with decreasing temperature.

From data for $YBa_2Cu_4O_8$(248) under pressure,[10] it appears that x is *not* a unique parameter for the crossovers in Fig. 1. The stochiometric compound 248 has a $T_c\approx80$ K and a resistivity with a crossover from $\sim T$ to a higher T dependence below about 200 K, very similar to the properties of $YBa_2Cu_3O_{6.7}$. Under pressure, T_c rises to 110 K at $P\simeq100$ kbar. Simultaneously the resistivity becomes linear down to T_c. The low-energy excitations also change under pressure. In 248 the Raman spectrum shows a low-energy decrease. Under pressure as resistivity becomes linear the low-energy spectrum is restored, becoming like that of the optimally doped $YBa_2Cu_3O_{6.9}$, i.e., frequency independent.[11]

The schematic phase diagram of Fig. 1 suggests that the anomalous normal state of region 1 (as well as superconductivity) is controlled by fluctuations around the point $x\approx x_c$ and $T\approx0$. This is consistent with the marginal Fermi-liquid (MFL) phenomenology[12] which suggests that the breakdown of Landau theory is due to scale-invariant fluctuations consistent with having a quantum critical point[13] (QCP) (i.e., a singularity at $T=0$) near the ideal composition. The critical point itself is inaccessible due to the superconductive instability.

The MFL has a single-particle self-energy of the form

$$\Sigma(\omega,q)=\lambda\left[\omega\ln\frac{\omega_c}{x}+ix\,\mathrm{sgn}\omega\right], \tag{1.1}$$

where $x=|\omega|$ for $|\omega|\gg T$ and $=\pi T$ for $T\gg|\omega|$; λ is a coupling constant and ω_c is a cutoff energy. The quasiparticle renormalization amplitude

$$z(\omega)=\left(1-\frac{\partial\mathrm{Re}\Sigma}{\partial\omega}\right)^{-1}=\left(1+\lambda\ln\frac{\omega_c}{x}\right)^{-1} \tag{1.2}$$

then vanishes logarithmically as $(\omega,T)\to0$.

A microscopic theory should specify the nature of the critical point and the symmetry on either side of it. It should also answer the following question: If there is a critical point at $x=x_c$, $T=0$, what about its continuation in the (x-T) plane? Should there not be evidence of nonanalytic properties on a line in the (x-T) plane? Experimentally, there is indeed a crossover in the properties in the (x-T) plane from region 1 to region 4 of Fig. 1. But why a crossover rather than a transition? Or is it that the properties studied such as transport and specific heat are often only weakly sensitive to a transition?

Equation (1) gives only the single-particle scattering rate τ_{sp}^{-1}. This was used to understand[12,14] the observed tunneling conductance $G(V)\sim|V|$ for $T\to0$ and to predict the line shapes in single-particle spectra.[15] A crucial aspect of the properties of the Cu-O metals is that the momentum transport scattering rates, measured in resistivity $\rho(T)$ [as well as in optical conductivity[16] $\sigma(\omega,T)$ and Raman cross section[17] $S_R(\omega,T)$], are also proportional to $\max(|\omega|,T)$. So is the energy scattering rate τ_{en}^{-1} measured by thermal conductivity $\kappa(T)$.[18] The experimental result that, at $(q,\omega)\to0$,

$$\tau_{\mathrm{sp}}^{-1}\sim\tau_{\mathrm{mom}}^{-1}\sim\tau_{\mathrm{en}}^{-1}\sim T \tag{1.3}$$

puts a strong constraint on theories. The single-particle scattering rate is required in general to be at least as singular as the momentum scattering rate τ_{mom}^{-1}. The immediate conclusion is that the experiments require $\mathrm{Im}\Sigma(\omega,k_F)\sim\omega^{\alpha}$, $\alpha\leqslant1$. Angle-resolved photoemission should be used to put stricter bounds on the single-particle self-energy than have been done so far. But an easier way might be through the electronic specific heat. The electronic specific heat is directly related to the exact single-particle Green's function. For the marginal case $\alpha=1$, $C_v\sim N(0)T(1+\lambda\ln\omega_c/T)$. A more singular self-energy $\alpha<1$ gives $C_v\sim N(0)T^{\alpha}$. In the experiments the electronic part of C_v is obtained only by subtracting the estimated phonon heat capacity and at $x\approx x_c$ is reported to be consistent with $\sim T$. While logarithmic corrections to it cannot be ruled out, substantial singular departures are ruled out.

The proportionality of the single-particle and the transport scattering rates occurs if the fluctuations leading to Eq. (1.1) are essentially momentum independent as suggested by the MFL phenemenology. (In that case there are no vertex corrections in the calculation of the conductivity. See further discussion in Sec. VII.) But this poses the serious dilemna that on the one hand we wish to be near a critical point, on the other that we need (nearly) momentum-independent fluctuations.

The trivial way to get Eq. (1.3) is if the experiments are in a temperature range $T\gtrsim\omega^*$ where ω^* is the characteristic frequency of some fluctuations which scatter the fermions. Then the density of such fluctuations is $\sim T$, giving Eq. (1.3).

This is ruled out by the specific heat (and magnetic susceptibility experiments) experiments.[4] If such fluctuations are of physical quantities like spin or density fluctuations of fermions, a characteristic enhancement in $\gamma = C_v/T$ of $O(E_F/\omega^*) \sim O(10^2)$ must occur as in the heavy fermion compounds. Experimentally, the specific heat and magnetic susceptibility at the ideal composition are consistent with Fermi-liquid behavior, $\sim T$ and constant, respectively, with no more than about a factor of 2 enhancements over noninteracting electrons in the measured temperature range. (The data, however, do allow for logarithmic or small power law corrections.) This as well as the fact that $\sigma(\omega,T)$ and $S_R(\omega,T)$ behaves smoothly in the range $\omega \lesssim T \lesssim \omega_c$ where $\omega_c \sim O(\frac{1}{2}\text{ eV})$ suggests that there is no low-energy scale near optimum doping and that the upper cutoff frequency of the fluctuations is very high, $O(\frac{1}{2}\text{ eV})$.

It is hard to imagine that the fluctuations due to the antiferromagnetic $T=0$ critical point at $x \approx 0.02$ can have much to do[19] with phenomena at $x \approx x_c$, with $x_c \gtrsim 0.15$. Temperature-independent magnetic correlation lengths of about 2 Å are observed at $x \approx x_c$ in $YBa_2Cu_3O_{6.93}$.[20] Temperature-dependent lengths of ~ 20 Å are observed in $La_{1.85}Sr_{0.15}CuO_4$,[21] but with less than $\sim 10\%$ of the total frequency-integrated spectral weight in the q-dependent part. The normal-state anomalies are identical in both compounds. Similarly, there is no evidence of any universal phase-separation fluctuations or charge density fluctuations[22,23] in different compounds at $x \approx x_c$. It would appear that if a critical point is responsible for the unusual metallic state, it must be associated with some quite unusual order parameter which is hard to detect.

Equations (1.1) and (1.3) cannot be used to understand the observed anomalies in NMR,[24] Hall effect,[25] and magnetoresistance.[26] In $YBa_2Cu_3O_{6.9}$, where band-structure calculations[27] give a very small usual Hall conductivity due to particle-hole symmetry, the Hall angle $\Theta_H = \sigma_{xy}/\sigma_{xx}$, with the magnetic field perpendicular to the plane, varies[25] approximately as T^{-2} between 100 and 300 K In the same range the normalized magnetoresistance $\Delta\rho(H)/\rho$ varies[26] roughly as T^{-4} with $\Theta_H^2/\Delta\rho/\rho \approx 0(1)$. The Hall-effect data[25(b)] in $La_{2-x}Sr_xCuO_4$, however, appears more complicated where a saturation in the anomalous contribution occurs at temperatures below about 60 K. In view of this, it is not clear at the moment whether the Hall-effect anomaly is a leading low-temperature singularity or an intermediate- to high-temperature phenomena. It is worth noting that a singularity in the Hall angle $\sim T^{-2}$, equivalently a Hall number diverging as T^{-1}, implies a spontaneous Hall effect in the limit $T \to 0$, i.e., a Hall voltage in the absence of a magnetic field. Kotliar *et al.*[28] have found this behavior in a solution of the Boltzmann equation which, besides a scattering rate $\tau_{\text{mom}}^{-1} \sim T$, contains a phenomenological skew scattering rate proportional to the applied magnetic field which is $\sim T^{-1}$.

Perhaps the most astonishing of the normal-state anomalies are the nuclear relaxation rates $^{Cu}T_1^{-1}$ and $^{O}T_1^{-1}$ of copper and oxygen nuclei, respectively.[24] While $(^{Cu}T_1T)^{-1}$ appears to diverge as the temperature is decreased, suggesting singular *local* magnetic fluctuations at the Cu nuclei, $(^{O}T_1T)^{-1}$ is a constant, which is the conventional behavior. Furthermore, $(^{O}T_1TK)^{-1}$, where K is the measured Knight shift at oxygen, is a constant within 20%, irrespective of the compound studied or the density x in any given compound in the metallic range.[29] Other experiments show that copper and oxygen orbitals are well hybridized. Nevertheless, it appears that the local magnetic fluctuations at copper and oxygen sites are quite different.

It is axiomatic that the fluctuations responsible for the anomalous metallic state also are responsible for the instability to the superconducting state. The anomalous fluctuations develop a gap in the superconducting state as predicted[30] and observed in a wide variety of experiments on the quasiparticle relaxation rate deduced through transport experiments[31] and in angle-resolved photoemission experiments.[32] The symmetry of the superconducting state appears to be consistent with ''D wave'' (if the lattice is assumed tetragonal).[33] This issue is not completely settled yet.[34] Moreover, the electron-doped material $Nd_{2-x}Ce_xCuO_4$ appears to be an ''S-wave'' superconductor.[35]

To summarize, existing experiments require an *internally consistent* microscopic theory to

(i) reproduce the phase diagram of Fig. 1 with a non-Fermi-liquid metallic phase near the composition for the highest T_c with crossovers to a Fermi liquid on the high doping side. The underdoped regime should show a loss at low energies of both particle-hole excitations (in spin as well as charge channels) and of single-particle excitations, and a strong tendency to insulating behavior due to disorder;

(ii) have equilibrium properties such as specific heat and magnetic susceptibility near the ideal composition *consistent* in the measured range of T with characteristic Fermi-liquid behavior to within small corrections and in magnitude be within factors of $O(2)$ of those for noninteracting electrons;

(iii) have long-wavelength transport relaxation rates used to interpret electrical conductivity and thermal conductivity at the ideal composition that satisfy Eq. (3). At $x = x_c$ the fluctuations leading to the anomalous transport should have no scale other than a cutoff of the $O(1/2\text{ eV})$.

(iv) The fluctuations should have a symmetry such that they produce singular local magnetic fluctuations at copper nuclei to give the observed anomalies in the copper nuclei relaxation rate, but no singular local magnetic fluctuations at the oxygen nuclei.

(v) The fluctuations should be capable of producing a pairing instability of D-wave symmetry.

There are of course many other special properties discovered in a subject in which $O(5 \times 10^4)$ papers have been published. But I regard the requirements listed above as the most basic or a least the irreducible minimum. The theory developed in this paper attempts to meet these requirements and suggests a few crucial experiments.

B. Choice of a model

The choice of a model with which to do microscopic theory should be influenced by the fact that copper-oxide metals are unique. None of the thousands of transition-metal compounds studied share their properties. The point of view taken here and elsewhere[36] is that the unique properties of Cu-O metals arise from their unique chemistry in which

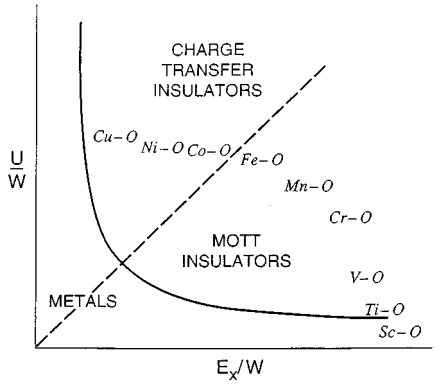

FIG. 2. The Zaanen-Sawatzky-Allen (ZSA) phase diagram for $3d$ transition-metal oxides, slightly modified and showing the schematic change in the position of the transition-metal oxides going from left to right of the periodic table. The modification is that one of the axes is the ionic energy E_x defined through particle-hole spectra. ZSA used the charge transfer gap Δ defined through one-particle spectra. $E_x<\Delta$ due to particle-hole interactions.

ionic interactions play a crucial *dynamical* role. This point has been extensively discussed[37] and will only be briefly repeated here. The divalent transition-metal oxides at 1/2 filling can be put on the diagram[38] in Fig. 2 in which one of the axes is the normalized local repulsion energy U on the transition metal (TM):

$$U/W=[E(\mathrm{TM})^{3+}+E(\mathrm{TM})^{1+}-2E(\mathrm{TM})^{2+}]/W, \tag{1.4}$$

where W is the bandwidth. The other axis is the *ionic energy*

$$E_x/W=[E(\mathrm{TM}^{1+}\mathrm{O}^{1-})-E(\mathrm{TM}^{2+}\mathrm{O}^{2-})]/W. \tag{1.5}$$

U is the energy to convert two transition-metal ions with formal charge state 2^+ to one with formal charge state 1^+ and the other to 3^+, while E_x is the energy to transfer charge from the ground-state configuration of a transition-metal ion with charge 2^+ and a nearest-neighbor oxygen ion with 2^- to a transition-metal ion with charge 1^+ and oxygen ion with charge 1^-. Screening and dipole corrections, etc., in the solid are included in the definitions of U and E_x.

As one moves from the left to the right of the periodic table, the ionization energy of the TM falls, thereby decreasing E_x/W relative to U/W with corresponding movement of Fig. 2. In the insulating state of Cu-O, E_x is only about 1 eV. It is a charge-transfer insulator with the lowest-energy one-particle spectra primarily on copper, $\mathrm{Cu}^{2+}\rightarrow\mathrm{Cu}^{+}$, while the one-hole spectra is primarily in oxygen, $\mathrm{O}^{2-}\rightarrow\mathrm{O}^{-}$; see Figs. 3(a) and 3(b) where the contrast to transition-metal oxides towards the left of the periodic table is also shown. In the metallic state, obtained by doping, there are charge fluctuations on copper and on oxygen of similar magnitude. $E_x\approx 1$ eV is made up of from two sets of energies, the atomic level energies and the Madelung or ionic energies, each of which is $O(10\text{ eV})$. Indeed all transition-metal oxides owe their structural stability to the ionic energies. But in the metallic state these energies have little dynamical role to play in most TM oxides because there are hardly any fluctuations on oxygen; i.e., although the ionic fluctuation energy term in the Hamiltonian

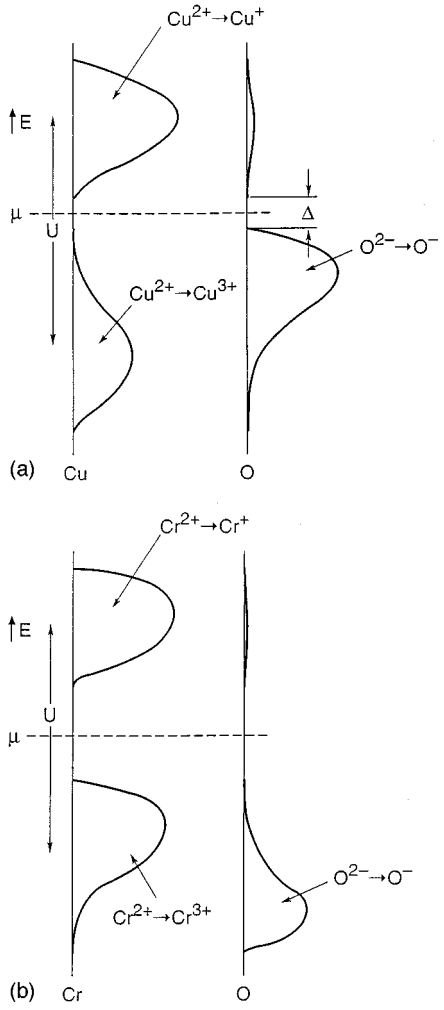

FIG. 3. (a) Schematic one-hole spectra (measured in photoemission) and one-particle spectra (measured in inverse photoemission) projected onto Cu states and oxygen states in Cu-O compounds at 1/2 filling. (b) Schematic one-hole spectra and one-particle spectra for a transition metal oxide far to the left of Cu, say, Cr-O, projected onto Cr and onto O.

$$\sum_{i<j} V_{ij}n_i n_j \tag{1.6}$$

has $\Sigma_{i<j}V_{ij}\sim O(10\text{ eV})$, the fluctuation δn_j on the oxygen ions requires a large energy and is insignificant. An effective low-energy Hamiltonian of the Hubbard form is then adequate. This is not true in the metallic state of Cu-O where $\langle\delta n_0\rangle/\langle n_0\rangle\sim O(1)$.

One of the aims of this paper is to show that finite-range interactions, if sufficiently strong, lead to qualitatively new features in the phase diagram of the model. The one-dimensional version of the model has been extensively investigated by numerical methods.[39] Bosonization methods give incorrect results for the model for V's$\gtrsim 0(E_x)$ whereas as is well known the one-dimensional (1D) Hubbard model can be bosonized for any value of U. Therein lies a clue to understanding how in one and higher dimension the low-energy properties of the model are quite different for small V and for large V. Bosonization is inherently a weak-coupling method; it works in the (1D) Hubbard model be-

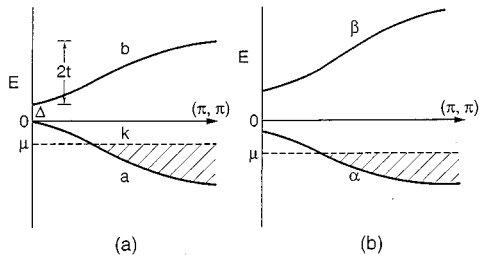

FIG. 4. The bonding b and the antibonding band a for the two-dimensional band structure from one-electron theory in the hole representation with chemical potential μ. Under the $q=0$ transition discussed in the text, identical internal rearrangements in each unit cell occur. So the band structure changes merely to the bands β and α shown.

cause the properties at weak coupling (small U/t) are *similar* to those at large coupling. The numerical results show a change in properties as V is varied; for $V \gtrsim 0(E_x)$ they show the charge-transfer instability described below, and growing superconducting correlation length as temperature is decreased, whereas bosonization methods find V's to be irrelevant. (One-dimensional models do not have some essential features, discussed below, of the model in higher dimensions.)

C. Preview of the properties of the model

In Sec. II we discuss that it is enough to consider a two-band model representing Cu and O bonding $-b$ and antibonding $-a$ bands (but with O-O hopping included) as illustrated in Fig. 4. In the hole representation, the chemical potential μ is in the lower band as shown. For noninteracting electrons μ would be in the middle of band a at 1/2 filling as in La_2CuO_4 or $YBa_2Cu_3O_6$. For hole doping, as for most Cu-O compounds, μ rises with doping x, for example, in $La_{2-x}Sr_xCuO_4$ or $YBa_2Cu_3O_{6+x}$. We will find it important to consider the most general form of two-body interactions allowed by symmetry in the space of these two bands. When the strength of the interactions is on the same scale as the overall electronic bandwidth every term has a crucial role to play.

If μ were in the gap between bands a and b, the model is identical to the excitonic insulator problem,[40] which has been extensively discussed. We investigate here the model with μ in one of the bands. This changes the problem substantively.

It is well known that interactions completely alter the one-electron picture at 1/2 filling; a gap develops around the chemical potential and the relative amount of Cu and O character of the occupied and unoccupied states is drastically altered. μ stays in the band significantly away from 1/2 filling but the relative Cu-O character of the occupied and unoccupied states is again expected to be quite different from the one-electron picture. If no change in the lattice symmetry occurs due to the interactions, this is formally describable by a $q=0$ instability of the one-electron band structure to a state in which

$$T_x \sim \mathrm{Re} \sum_{\mathbf{k}} \mathcal{F}_x(k) \langle a^\dagger_{\mathbf{k}\sigma} b_{\mathbf{k}\sigma} \rangle \neq 0. \tag{1.7}$$

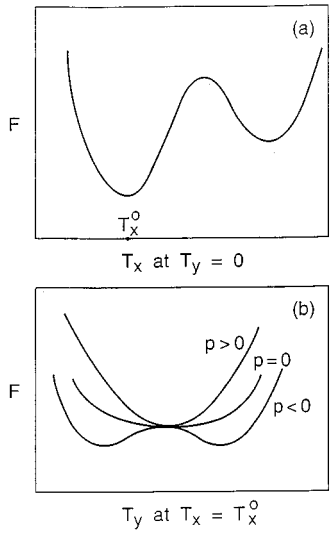

FIG. 5. (a) The calculated mean-field free energy as a function of the real part of interband order parameter T_x described in the text. (b) For a fixed $T_x = T_x^0$, the free energy as a function of the imaginary part of the interband order parameter T_y. T_y takes the value 0 for $p>0$ and a finite value below $p<0$ through a second-order transition. p is a parameter defined in terms of the parameters of the Hamiltonian and for a given compound can be varied by varying the electron density, temperature, or pressure. $T_y \neq 0$ corresponds to a circulating current pattern in the ground state shown in Fig. 10.

Here $\mathcal{F}_x(k)$ is a form factor expressing the relative Cu and O character of states in bands a and b. We will see that T_x is closely related to the relative average charge in Cu and O orbitals. The mean-field free energy as a function of T_x is shown in Fig. 5(a). With $T_x \neq 0$, the orbitals must be rehybridized, leading to new bands α and β of the same general form as a and b, as shown in Fig. 4. This is expected to occur for strong interactions at very high temperatures for all x of interest just as it does at $x=0$. For the most general interactions, such a transition is of first order, as for a free energy of the form shown in Fig. 5(a). Previous investigations[41,42] of the model had focused on this charge-transfer instability.

We show that the model also has an interesting second-order transition in the Ising class to a state in which

$$T_y \sim \mathrm{Im} \sum_{\mathbf{k}\sigma} \mathcal{F}_y(k) \langle a^\dagger_{\mathbf{k}\sigma} b_{\mathbf{k}\sigma} \rangle \neq 0. \tag{1.8}$$

The mean-field free energy, for a fixed $T_x \neq 0$, as a function of T_y for various values of a parameter p which is a function of x and T is shown in Fig. 5(b). This transition therefore occurs on a line $T_c(x)$ in the x-T plane. We will be specially interested in the properties in the vicinity of the point $x = x_c(0)$ where $T_c = 0$ which we identify as the quantum critical point.[43]

A finite T_y provides an additional relative phase to the wave functions at Cu and the two O sites in a unit cell. We will see that the ground state with a finite T_y corresponds to a fourfold pattern of circulating current within a unit cell with all cells staying equivalent. This is illustrated in Fig. 6. We may call it the circulating current (CC) phase. Transla-

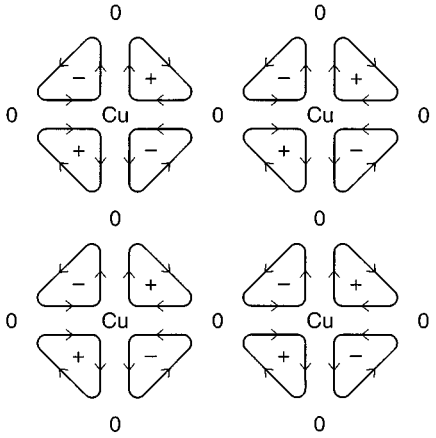

FIG. 6. The deduced ground-state current distribution pattern in the circulating current phase drawn for four cells. The + and − signs indicate magnetic fields pointing up and down.

tional symmetry is preserved but time-reversal invariance and fourfold rotational symmetry are broken. The product of the time reversal and the fourfold rotation is preserved.

The pattern shown in Fig. 6 breaks a twofold symmetry—the +'s and the −'s could be reversed uniformally. This is possible to understand from Fig. 7 which gives the relative phases of the Cu-$d_{x^2-y^2}$ and O -p_x and p_y orbitals in a unit cell at $k=0$. The Hamiltonian has the twofold symmetry that given the phases of the two p_x orbitals the phases of the two p_y orbitals can be reversed. This symmetry is broken by the circulating current phase.

In connection with the excitonic insulator problem and the Hubbard model at 1/2 filling circulating current phases have also been discussed, which also break translational symmetry, and go by the names of orbital antiferromagnets[44] or staggered flux phases.[45] There are two important differences, because of which the present work meets requirements (i) through (v) above and thus qualifies as a serious candidate for the theory of the Cu-O metals. (i) Our use of a Cu-O model with more than two atoms per unit cell allows a $q=0$ transition to a circulating current phase, so that lattice translation symmetries are preserved. There is no change in the symmetry of the band structure. (ii) We discuss such a phase in the metallic state. This leads to a very special nature of the collective fluctuations near the QCP due to scattering of the fluctuations by low-energy particle-hole excitations at the Fermi surface. The problem of determining the spectrum of the fluctuations is the same as the absorption in a degenerate semiconductor with finite-mass electrons and holes and in the limit that the interactions are much larger than the Fermi energy. We show that the logarithm of the frequency of the fluctuations scales with their momentum; i.e., the QCP has a dynamical critical exponent $z_d=\infty$. The fluctuations are thus independent of momentum to a logarithmic accuracy. This extreme quantum limit is essential to understand the observed behavior in long-wavelength, low-frequency transport properties summarized by Eq. (1.3) and its finite-frequency counterparts.

The model is stated more completely in Sec. II. One can study the model as interactions are increased from zero or take a strong-coupling point of view and consider corrections about an infinite value of the interactions. Both approaches

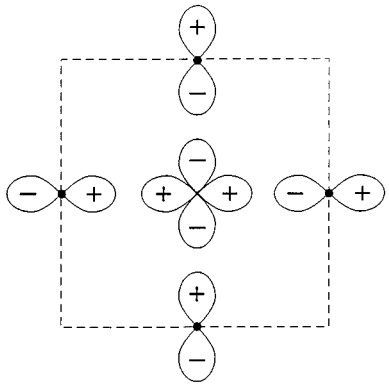

FIG. 7. The unit cell of Cu-O compounds in the x-y plane and the minimal orbital set: $d_{x^2-y^2}$ orbital of Cu and a p_x and a p_y orbital of oxygen per unit cell. A particular choice of the relative phases of the orbitals at $\mathbf{k}=0$ is shown.

lead to the same ''intermediate-energy-scale'' Hamiltonian whose analysis begins in Sec. V. Section III is devoted to the strong-coupling expansion. The low-energy Hamiltonian is derived and analyzed in Secs. V and VI where it is shown that a systematic and controlled analysis is possible. The physical properties of the pure model are investigated in Sec. VII, and in Sec. VIII a beginning is made to consider the effect of impurities in the properties of the model. Impurities are strongly relevant near a $z_d=\infty$ transition. For arbitrarily small concentration, they convert the line $T_c(x)$ to a crossover. We also show that for an arbitrarily small concentration of impurities in a non-Fermi liquid, the Fermi surface withers away at low temperatures. The density of states at the chemical potential is zero and the resistivity is infinity as $T\rightarrow 0$ (unless superconductivity intervenes).

Not including the effect of disorder the schematic-deduced phase diagram of the model is shown in Fig. 8. In region I, the properties are determined by quantum fluctuations and are that of a marginal Fermi liquid with a crossover to a Fermi-liquid regime in region III. In region II, $T_y\neq 0$ in the pure limit. This phase should have Fermi-liquid properties at low temperatures in the pure limit but with different parameters from that of region III. The transition between regions I and II turns into a crossover at an arbitrarily small concentration of impurities. At low temperatures impurities are expected to lead to a further crossover in region III to an

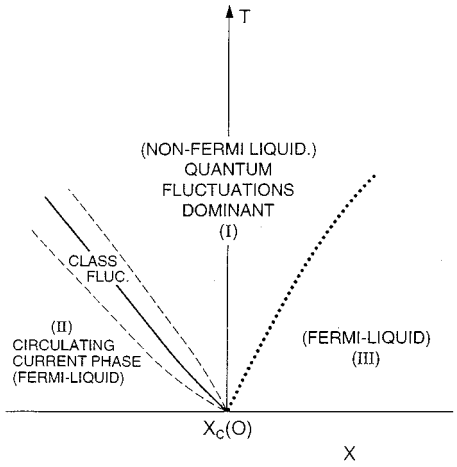

FIG. 8. The theoretical phase diagram in the pure limit. The effect of impurities is discussed in the text.

insulating regime with a zero density of states at the chemical potential. The antiferromagnetism phase near 1/2 filling and the superconductivity phase near x_c which are also properties of the model are not shown.

In Sec. IX, a beginning is made to study the pairing instability due to the exchange of the circulating current fluctuations and a propensity towards a ''D-wave'' superconducting instability is indicated.

In Sec. X the shortcomings of the theoretical calculations as well as the unexplained features of the experiments are highlighted. Experiments are suggested to test several features of the theoretical proposal. The most important is to observe the current pattern of Fig. 6 by polarized-neutron or x-ray scattering.

II. MODEL FOR COPPER OXIDES

The basic building block of the Cu-O compounds is the elongated CuO_6 octahedra in which the planar short bond oxygens are shared at the corners to produce a layered, anisotropic three-dimensional structure. The interlayer kinetic energy depends on the details of the structure. In the least anisotropic compounds the interlayer bandwidth is $O(10^{-1})$ of the intralayer bandwidth. Since the properties of such compounds in the temperature region of the normal state are the same as of those with anisotropy ratio $O(10^{-4})$, a two-dimensional model is appropriate for the essential physics. The basis set for the minimum Hamiltonian is the $d_{x^2-y^2}$ orbital on the Cu ions and the p_x and p_y orbitals on the O ions; see Fig. 8. In this basis set the Hamiltonian is written as

$$H=H_0+H_1+H_2. \tag{2.1}$$

H_0 is the kinetic energy:

$$H_0=\sum \frac{\Delta_0}{2}(n_{di}-n_{pxi}-n_{pyi})-\mu(n_{di}+n_{pxi}+n_{pyi})+\sum_{i,\sigma} t_{pd}d^{\dagger}_{\sigma i}(p_{x,i+a/2,\sigma}-p_{x,i-a,\sigma}+p_{y,i+a/2,\sigma}-p_{y,i,-a/2,\sigma})$$
$$+t_{pp}p^{\dagger}_{x,i+a,\sigma}(p_{y,i+a/2,\sigma}-p_{y,i-a/2,\sigma})+\text{H.c.} \tag{2.2}$$

Here (i) sums over the unit cells in the plane, $d^{\dagger}_{i\sigma}$ refers to the Cu d orbitals, and $p_{(x,y),i\pm a/2,\sigma}$ to the oxygen p_x or p_y orbitals, which are neighbors to Cu in cell i at a distance $a/2$. The relative signs in the kinetic energy take into account the phases of the orbitals, as shown in Fig. 7.

H_1 is the short-range part of the interactions

$$H_1=\sum_{i,\sigma} U_d n_{di\sigma}n_{di\bar{\sigma}}+U_p n_{pi\sigma}n_{pi\bar{\sigma}}. \tag{2.3}$$

H_2 is the long-range part of the electron-electron interactions and the exchange interaction important only for nearest neighbors:

$$H_2=\sum_{i,j} V_{ij}n_i n_j+\sum_{(i,j)} V_x \mathbf{s}_i\cdot\mathbf{s}_j, \tag{2.4}$$

where $n_i=n_{di}$ or $n_{px,i}$, $n_{py,i}$ as appropriate. One must include the long-range $V_{ij}\sim|\mathbf{R}_i-\mathbf{R}_j|^{-1}$ for $|\mathbf{R}_i-\mathbf{R}_j|\to\infty$ to keep the long-wavelength charge oscillations at a finite plasma frequency. Otherwise, only the nearest-neighbor Cu-O and O-O V_{ij} need be considered.

Diagonalization of H_0 gives the model ''one-electron'' band structure, which has ''Cu-O bonding'' and ''antibonding bands'' and a O-O ''nonbonding band.'' For $t_{pp}=0$, the bonding band $-b$ and the antibonding band $-a$ are decoupled from the nonbonding band. $t_{pp}\neq 0$ is important for the results of this paper, but I consider only the bonding and the antibonding for simplicity and neglect the nonbonding band. The eigenvalues and eigenvectors of the bands kept must include the effects of t_{pp}. It will be clear that smaller interactions are needed in the three-band model than in the simplified model for the important instabilities derived in Sec. IV.

The dispersion of the bands a and b will be denoted by $\epsilon_a(\mathbf{k})$ and $\epsilon_b(\mathbf{k})$. These are sketched in Fig. 4. Expressions for them, derived perturbatively in t_{pp}/t_{pd}, are given in Appendix A. Their eigenvectors are specified by the annihilation operators for states in them in terms of annihilation operators for d and $p_{x,y}$ orbitals at lattice sites:

$$a_{\mathbf{k}\sigma}=u_{ad}(\mathbf{k})d_{\mathbf{k}\sigma}+u_{ax}(\mathbf{k})\sin\left(\frac{k_x a}{2}\right)p_{x\mathbf{k}\sigma}+u_{ay}(\mathbf{k})\sin\left(\frac{k_y a}{2}\right)p_{y\mathbf{k}\sigma}, \tag{2.5a}$$

$$b_{\mathbf{k}\sigma}=u_{bd}(\mathbf{k})d_{\mathbf{k}\sigma}+u_{bx}(\mathbf{k})\sin\left(\frac{k_x a}{2}\right)p_{x\mathbf{k}\sigma}+u_{by}(\mathbf{k})\sin\left(\frac{k_y a}{2}\right)p_{y\mathbf{k}\sigma}, \tag{2.5b}$$

where

$$d^{\dagger}_{\mathbf{k}\sigma}=\frac{1}{\sqrt{N}}\sum_i d^{\dagger}_{i\sigma}e^{i\mathbf{k}\cdot\mathbf{R}_i},$$

$$p^{\dagger}_{x(y)\mathbf{k}\sigma}=\frac{1}{\sqrt{N}}\sum_i p^{\dagger}_{ix(y)\sigma}e^{i\mathbf{k}\cdot\mathbf{R}_i}.$$

i label the unit cells; the Cu atom in the unit cell i is taken to be at $\mathbf{R}_i$. Expressions for these coefficients, also calculated perturbatively in t_{pp}/t_{pd}, are given in Appendix A.

Band-structure calculations give $t_{dp}, 2t_{pp}, \Delta_0 \sim O(1\text{ eV})$; various spectroscopic methods give the local repulsion on Cu: $U \sim O(10\text{ eV})$. As good an estimate of the nearest-neighbor Cu-O repulsion as any is

$$V_{\mathrm{NN}} \gtrsim e^2/[\epsilon(1\text{ eV})R_0], \tag{2.6}$$

where R_0 is 1/2 the unit cell size and $\epsilon(1\text{ eV})$ is the measured long-wavelength di-electric constant at an energy of $O(1$ eV), which is ≈ 4. This gives the nearest-neighbor Cu-O interaction $\gtrsim 1.7$ eV. So multiplied by the number of neighbors and considering polarization corrections, etc., the characteristic Madelung energies controlling Cu-O charge fluctuations is also of $O(10$ eV). Calculations of Madelung energies[46] in the actual lattice support this estimate.

The interaction energies and the overall electronic bandwidth are therefore of the same order. We can directly project the Hamiltonian (2.1) onto the basis set of the bonding and antibonding k-space orbitals obtained by diagonalizing Eq. (2.2). This results in the most general two-band Hamiltonian allowable by symmetry. Such a Hamiltonian (projected to interactions in the spin-singlet channel, which alone is important) is given in Eq. (4.1). The reader may at this point skip directly to Eq. (4.1) and the subsequent analysis. Although this approach is quite consistent for the metallic state, it is hard to derive the insulating phase near 1/2 filling from such a basis or to see that, although the low-energy physics at 1/2 filling of the general model is identical to the Hubbard model, it may not be so in the metallic state. A basis of local real-space orbitals constructed in the strong-coupling limit to suppress some of the charge fluctuations is more convenient. The next section is devoted to deriving the projections of the Hamiltonian (2.1) to such a basis. The subsequent analysis, which is a simple generalization of slave boson methods,[47] yields the Hamiltonian (4.1) as well. The results of this paper are qualitatively similar starting from either end in the ratio of interaction energy to the one-particle bandwidth.

III. STRONG-COUPLING LIMIT

It is convenient to rewrite the Hamiltonian as an intracell part and an intercell part to calculate in the strong-coupling limit. We define a linear combination $D^\dagger_{i\sigma}$ of operators on oxygen orbitals in a cell i which hybridize with the $d_{x^2-y^2}$ orbital in the same cell:

$$D^\dagger_{i\sigma} = \frac{1}{\sqrt{4}}(p_{i+a_x} - p_{i-a_x} + p_{i+a_y} - p_{i-a_y}). \tag{3.1}$$

$D^\dagger_{i\sigma}$ creates an orbital which also transforms as a $d_{x^2-y^2}$ orbital about the center of the cell i. In the geometry of the Cu-O lattice the orbitals created by $D^\dagger_{i\sigma}$ are not orthogonal for near-neighbor i. Wannier orbitals can be defined which are orthogonal for different i. Such orbitals can be expressed as a linear combination of the orbitals created by $D^\dagger_{i\sigma}$.

H_0 can be reexpressed as

$$H_0 = H_{0,\mathrm{cell}} + H_{0,\mathrm{intercell}}, \tag{3.2}$$

where because there is no hybridization at the zone center

$$H_{0,\mathrm{cell}} = \sum_i \Delta_0(n_{di} - n_{Di}). \tag{3.3}$$

We write the kinetic energy completely generally as

$$H_{0,\mathrm{intercell}} = \sum_{(ij),\sigma,\mu\nu} t_{i\mu,j\nu}(\mu^\dagger_{i\sigma}\nu_{j\sigma} + \mathrm{H.c.}), \tag{3.4}$$

so that it reproduces the one-electron bonding and antibonding bands. Here (μ,ν) sum over d or D. The use of nonorthogonal orbitals makes t_{ij} nonzero over a range larger than nearest neighbors. This conflict between the necessity of using nonorthogonal orbitals to handle strong local, but not just on-site, interactions and Bloch waves for a periodic lattice appears unavoidable. We need not dwell on this because the final projected Hamiltonian (4.1) for further analysis depends only on symmetry.

The interaction terms H_1 and H_2 remain of the same general form in terms of $D_{i\sigma}$'s as in Eq. (2.3) and Eq. (2.4) with a redefinition of coefficients. We will simply regard that the interaction terms have been rewritten in terms of D's, without changing the notation for the new coefficients.

A. States in the strong-coupling limit

The low-energy Hamiltonian for this model will now be derived. Since some of the important interactions are intracellular, we specify a basis set in terms of the states of a cell by cutting off the kinetic-energy connection between cells and the long-range Coulomb interactions.

Consider an average occupation of $(1+x)$ holes per unit cell as required by $(1+x)$ negative charges per unit cell assumed uniformly distributed by imposing a chemical potential μ. The minimum *low-energy* basis must then include states with one hole and with two holes per unit cell.

We define the *zero-hole state* $\phi^\dagger_{0i}|0\rangle$ as the closed-shell (spin zero) configuration in which the charge state of all oxygen ions is O^{2-} and of all copper ions is Cu^+.

One-hole states: These are of two kinds.

(i) $d^\dagger_{1\sigma i}|0\rangle$: a hole in the Cu $d_{x^2-y^2}$ orbital with energy $\Delta_0 - \mu$. Chemically, this is the spin-1/2 state $Cu^{2+}O^{2-}$ which is the nominal ground-state configuration of the insulator.

(ii) $d^\dagger_{2\sigma i}|0\rangle$: a hole in the orbital created by $D^\dagger_{i\sigma}$, i.e., the oxygen d orbital, with energy $-\Delta_0 - \mu$. (If such an orbital were localized on one atom, the charge configuration would be Cu^+O^-.)

Lowest-energy two-hole states $\phi^\dagger_i|0\rangle$: The lowest-energy two-hole state is the spin-singlet state with one hole in the Cu d orbital and the other in the oxygen d orbitals. The energy of this state is $E_\phi \equiv V - 2\mu$. (If the latter were confined to one atom, the charge configuration would be Cu^+O^-.) $\phi^\dagger_i$ should be thought of as a hard-core boson operator.

Neglected states: These are the following.

(i) Two holes in the bonding combination of oxygen orbitals with energy $-2\Delta_0 - 2\mu + U_p$. No essential physical difference arises if we include these two-hole states also in the low-energy sector.

(ii) Triplet state with one hole on Cu d and the other on the oxygens. This is above $\phi_i^\dagger|0\rangle$ by the exchange energy V_x, which is $O(V_{ij})$ for (ij) nearest neighbors.

(iii) Two holes on the Cu d orbitals with energy $2\Delta_0 - 2\mu + U_d$.

(iv) Three or a higher number of holes per unit cell.

(v) The zero-hole state $\phi_{0i}^\dagger|0\rangle$ with energy 0.

At low energies, the allowed cells in a cell i must fulfill the completeness relation or constraint

$$\psi_i^\dagger \psi_i + \phi_i^\dagger \phi_i = 1, \tag{3.5}$$

where $\psi_i \equiv (d_{1\uparrow}\ d_{1\downarrow}\ d_{2\uparrow}\ d_{2\downarrow})_i$. It is convenient to introduce Pauli matrices $\boldsymbol{\sigma}$ and $\boldsymbol{\tau}$ to specify, respectively, the spin $(\uparrow\ \downarrow)$ degree of freedom and the orbital (1 2) degree of freedom in the one-hole sector of the problem.

To derive a low-energy Hamiltonian, we must project Eq. (2.1) to states which fulfill the constraint (3.5). To this end, the bare operators $d_{i\sigma}$ and $D_{i\sigma}$ are expressed in terms of the constrained operators through the identities

$$d_{i\sigma}^\dagger = \frac{1}{\sqrt{2}}\ \phi_i^\dagger d_{2i-\sigma} \mathrm{sgn}\sigma, \tag{3.6}$$

$$D_{i\sigma}^\dagger = \frac{1}{\sqrt{2}}\ \phi_i^\dagger d_{1i-\sigma} \mathrm{sgn}\sigma. \tag{3.7}$$

The *intracell* terms are transformed by noting that

$$n_{di\sigma} = n_{1i\sigma} + n_{\phi i/2}, \tag{3.8}$$

$$n_{D_{i\sigma}} = n_{2i\sigma} + n_{\phi i/2}, \tag{3.9}$$

where

$$n_{1\sigma} = d_{1\sigma}^\dagger\ d_{1\sigma},\ \text{etc.},\quad \text{and}\quad n_{\phi_i} = \phi_i^\dagger \phi_i. \tag{3.10}$$

B. Hamiltonian in the strong-coupling limit

In terms of allowed states in the cell,

$$V_0 n_{di} n_{Di} = V_0 n_{\phi i} \tag{3.11}$$

and, for $i \neq j$,

$$V_{ij} n_{di} n_{Dj} = V_{ij}(n_{1i}n_{2j} + n_{\phi i}n_{\phi j} + n_{1i}n_{\phi j} + n_{\phi i}n_{2j}). \tag{3.12}$$

The term $\Sigma_j V_{ij} n_{1i} n_{2j}$ is assumed to be already included in the definition of the difference Δ_0 of the one-hole states. Summing over i and j and using Eq. (3.5) the last two terms cancel the second term and renormalize E_ϕ. In general, the interactions of the d_1 state and the d_2 state with the neighbors are different and symmetry allows terms of the form

$$\sum_{(i,j)} \overline{V_{ij}}(n_{1i} - n_{2i}) n_{\phi j}. \tag{3.13}$$

These renormalize Δ_0 downward proportionally to the density of two-hole states as found in Hartree-Fock and other previous calculations.[41,42]

Equation (3.3) is simply

$$H_{0,\mathrm{cell}} = \Delta_0 \sum_i\ (n_{1i} - n_{2i}). \tag{3.14}$$

Consider now the intercell part of the kinetic energy. Starting from a configuration obeying the constraint, the intercell kinetic energy leads to configurations which preserve the constraint as well as those that do not. Consider first the former. These are necessarily processes which alter the two-hole occupation in cell i and one-hole occupation in cell j to one hole in i and two hole in j or vice versa, for example,

$$\phi_i^\dagger d_{1j\sigma}^\dagger|0\rangle \rightarrow d_{2i\sigma}^\dagger \phi_j^\dagger|0\rangle. \tag{3.15}$$

Therefore, Eq. (3.4) projected to the lower-energy states gives (with $t_{ij} \equiv t_{id,jD}$)

$$H_{0,\mathrm{intercell}} = \sum_{(ij),\sigma,\mu\nu} t_{i\mu,j\nu}(\phi_i^\dagger d_{\mu\sigma i} d_{\nu\sigma j}^\dagger \phi_j + \mathrm{H.c.}). \tag{3.16}$$

The kinetic energy also operates on the one-hole states of neighboring cells i and j, creating disallowed states $\phi_{0i}^\dagger$ and the disallowed two-hole states on j. Eliminating such a kinetic energy term by a *canonical transformation* leads to an effective low-energy interaction in the space of the allowed one-hole states. This process is similar to that by which a Heisenberg exchange Hamiltonian is generated from the Hubbard Hamiltonian.[48] The new feature here is that the one-hole sector has a $\boldsymbol{\tau}$ degree of freedom as well as a $\boldsymbol{\sigma}$ degree of freedom. So there is an exchange in $\boldsymbol{\tau}$ space as well as $\boldsymbol{\sigma}$ space. The one-band Hubbard model produces an isotropic exchange Hamiltonian because the full Hamiltonian is invariant to spin rotations. This is again true in $\boldsymbol{\sigma}$ space here, but not in $\boldsymbol{\tau}$ space. The eigenvectors of the pseudospin $\boldsymbol{\tau}$ have in general different local energies, $\Delta \neq 0$ in Eq. (3.14) and different transfer integrals. Also, there are very many different intermediate states with no obvious rotational invariance. Here we derive the form of the effective interaction Hamiltonian from completely general considerations. An explicit derivation with calculation of the coefficients is given in Appendix B.

The intracell kinetic energy terms in Eq. (3.4) which connect the allowed one-hole states to the disallowed states may be written in terms of products of operators

$$\phi_{0i}^\dagger d_{\alpha\sigma i},\quad \phi_{2\mu j}^\dagger d_{\alpha\sigma j},\quad \alpha = 1,2, \tag{3.17}$$

where $\phi_{0i}^\dagger$ creates the zero-hole state and $\phi_{2\mu i}^\dagger$ creates one of the disallowed two-hole states labeled by μ. The canonical transformation consists in eliminating the intermediate states $\phi_{0i}^\dagger \phi_{2\mu j}^\dagger$ (where now the allowed two-hole state $\phi_j^\dagger$ is included in μ). The most general *pairwise* effective Hamiltonian is the sum over products of two kinetic energy operators with appropriate energy denominator. It has the general form

$$H_{\mathrm{int}} = \sum_{ij}\ J_{ij} \sum_{\sigma,\tau}\ (x_\tau \psi_{i\sigma\tau}^\dagger \psi_{j\sigma\tau}) \sum_{\sigma',\tau'}\ (x_{\tau'} \psi_{j\sigma'\tau'}^\dagger \psi_{i\sigma'\tau'}), \tag{3.18}$$

where ($\sigma=\uparrow,\downarrow$) and $\tau=(d_1,d_2)$. In Eq. (2.23), $J_{ij}x_\tau x_{\tau'}$ is the sum over intermediate high-energy (disallowed) states of matrix elements to such states divided by the corresponding energy denominators.

Equation (3.18) can be rewritten as

$$H_{\rm int}=-\sum_{ij} J_{ij}(1/4-\boldsymbol{\sigma}_i\cdot\boldsymbol{\sigma}_j)(\mathbf{A}/4-\boldsymbol{\tau}_i\mathbf{A}\boldsymbol{\tau}_j). \quad (3.19)$$

The Hamiltonian is isotropic in $\boldsymbol{\sigma}$ space and $\mathbf{A}$ expresses the anisotropy in $\boldsymbol{\tau}$ space:

$$A_{\tau\tau'}=x_\tau x_{\tau'}. \quad (3.20)$$

In Eq. (3.19),

$$\tau_{zi}=(d_1^\dagger d_1-d_2^\dagger d_2)_i, \quad (3.21)$$

$$\tau_{xi}=(d_1^\dagger d_2+d_2^\dagger d_1)_i \quad (3.22)$$

$$\tau_{yi}=i(d_1^\dagger d_2-d_2^\dagger+d_1)_i. \quad (3.23)$$

With axes defined as in Eqs. (3.21)–(3.23) the most general form of $\mathbf{A}$ is such as to generate

$$H_{\rm int}=H_{xy}+H_{\rm anis}, \quad (3.24)$$

$$H_{xy}=[J_{zz}\tau_z^i\tau_z^j+J_\perp(\tau_+^i\tau_-^j+\text{H.c.})](1/4-\boldsymbol{\sigma}_i\cdot\boldsymbol{\sigma}_j), \quad (3.25)$$

$$H_{\rm anis}=[J_{zx}(\tau_x^i\tau_x^j+\tau_x^i\tau_z^j)+J_\perp'(\tau_+^i\tau_+^j+\tau_-^i\tau_-^j)](1/4-\boldsymbol{\sigma}_i\cdot\boldsymbol{\sigma}_j). \quad (3.26)$$

The only conceivable terms missing in Eqs. (3.24)–(3.26) are those linear in τ_y. Note that $\tau_{yi}=i(D_i^\dagger d_i-d_i^\dagger D_i)$. Therefore (remembering that D_i and d_i refer to wave functions at different points in the unit cell i) τ_{yi} represents a current distribution within the unit cell i. Terms linear in τ_{yi} cannot be generated from a time-reversal-invariant Hamiltonian. Another way of seeing this is that if one has two bands as in Fig. 4 whose states are created by linear combination of operators $a_i^\dagger$ and $b_i^\dagger$, respectively, the most general two-body interactions (with operators on sites i and j) are (ignoring spin)

$$a_i^\dagger a_j^\dagger a_j a_i,\quad b_i^\dagger b_j^\dagger b_j b_i,\quad a_i^\dagger b_j^\dagger b_j a_i,$$
$$a_i^\dagger b_j^\dagger a_j b_i,\quad a_i^\dagger a_j^\dagger b_j b_i,$$
$$a_i^\dagger a_j^\dagger a_j b_i,\quad b_i^\dagger b_j^\dagger b_j a_i,$$

plus Hermitian conjugates of these. The terms in the first line can be rewritten in terms of $\tau_z^i\tau_z^j$, in the second line in terms of $(\tau_+^i\tau_-^j+\text{H.c.})$ and $(\tau_+^i\tau_+^j+\text{H.c.})$, and those in the third line in terms of $(\tau_{zi}\tau_{xj}+\text{H.c.})$ just as in Eqs. (3.24)–(3.26).

At 1/2 filling, $x=0$, the state $d_{2\sigma i}^\dagger|0\rangle$ is not allowed in the low-energy subspace. Then $\psi_i\equiv(d_{1\uparrow}d_{1\downarrow})$ only, and the low-energy Hamiltonian is obtained by dropping the $\boldsymbol{\tau}$ dependence in Eq. (2.24). The familiar Heisenberg Hamiltonian is then obtained. If one drops the $\boldsymbol{\tau}$ variable in the metallic state as well, the familiar t-J Hamiltonian derivable from the Hubbard model in the strong-coupling limit is obtained. As discussed in the Introduction, this is not justifiable for the parameters of the Cu-O problem. The $\boldsymbol{\tau}$ degrees of freedom make the problem richer and afford the possibility of new physics pursued in this paper.

At this point it is useful to collect all the terms of the effective Hamiltonian

$$H=\sum_i\left(\Delta_0+\sum_j V_{ij}n_{\phi j}\right)(n_{1i}-n_{2i})$$
$$-\sum_i\lambda_i(n_{1i}+n_{2i}+n_{\phi i}-1)-\mu\sum_i(n_{1i}+n_{2i}+n_{\phi i})$$
$$+H_{0,\rm intercell}+\sum_i E_\phi n_{\phi i}+H_{\rm int}. \quad (3.27)$$

λ_i enforces the constraint and μ is introduced to fix the hole density at $(1+x)$. $H_{\rm int}$ is given by Eqs. (3.24)–(3.26).

C. Mean field for the slave bosons

We look for uniform mean-field solutions

$$\lambda_i=\langle\lambda_i\rangle=\lambda, \quad (3.28)$$

$$\phi_i=\langle\phi_i\rangle=\phi. \quad (3.29)$$

We also look for spin-singlet solutions in the bonds $(i-j)$ favored by the kinetic energy term in Eq. (3.27) and the decomposition:[49]

$$J\left(\sum_{\sigma,\tau}x_\tau\psi_{i\sigma\tau}^\dagger\psi_{j\sigma\tau}\right)\left(\sum_{\sigma'\tau'}x_{\tau'}\psi_{j\sigma'\tau'}\psi_{i\sigma'\tau'}\right)$$
$$\approx\epsilon_{ij}\left(\sum_{\sigma\tau}x_\tau\psi_{i\sigma\tau}^\dagger\psi_{j\sigma\tau}\right)+\epsilon_{ij}^2/4J_{ij}, \quad (3.30)$$

where

$$\epsilon_{ij}=2J_{ij}\left\langle\sum_{\sigma,\tau}x_\tau\psi_{i\sigma\tau}^\dagger\psi_{j\sigma\tau}\right\rangle \quad (3.31)$$

are mean-field amplitudes.

The other decomposition of the interaction term in which mean-field amplitudes for $\boldsymbol{\tau}_i$ are introduced is more important to us. Note that given spin singlets in the bonds $(i-j)$, uniform spatial solutions in τ space are favored by the interactions in Eq. (3.24), for $J_\perp>J_\perp'$.

We now diagonalize the bilinear terms in τ space, i.e. the first five terms in Eq. (3.27), and transform to k space. This introduces bands a and b. Let $a_{k\sigma}^\dagger$, $b_{k\sigma}^\dagger$ create particles in these bands:

$$a_{\mathbf{k}\sigma}=u_{\mathbf{k}}d_{1\mathbf{k}\sigma}+v_{\mathbf{k}}d_{2\mathbf{k}\sigma}, \quad (3.32)$$

$$b_{\mathbf{k}\sigma}=-v_{\mathbf{k}}d_{1k\sigma}+u_{\mathbf{k}}d_{2\mathbf{k}\sigma}, \quad (3.33)$$

$$v_{\mathbf{k}}/u_{\mathbf{k}}=\tan[\tfrac{1}{2}\tan^{-1}\tilde{t}_{\mathbf{k}}/\Delta], \quad (3.34)$$

$$\tilde{t}_{\mathbf{k}}=t_{\mathbf{k}}\phi^2, \quad (3.35)$$

and

$$\Delta=(\Delta+\overline{V\phi}^2). \quad (3.36)$$

Here $t_{\mathbf{k}}$ is the lattice momentum transform of t_{ij}. The effective Hamiltonian projected to the bands a and b is given by Eq. (4.1). We denote the dispersion of the two bands due to this diagonalization also by $\epsilon_{\mathbf{k}a}$ and $\epsilon_{\mathbf{k}b}$. They have the symmetry properties of the band structure in the one-electron approximation, i.e., Eq. (2.5).

IV. ANALYSIS OF THE TWO BAND HAMILTONIAN

In the strong-coupling limit the *intermediate*-energy-scale Hamiltonian obtained from Eq. (3.27) after Eqs. (3.28) and (3.29) is

$$H=-(\lambda+\mu-1)\sum_{\mathbf{k}\sigma}(a^{\dagger}_{\mathbf{k}\sigma}a_{\mathbf{k}\sigma}+b^{\dagger}_{\mathbf{k}\sigma}b_{\mathbf{k}\sigma})-(\lambda+\mu-E_{\phi})n_{\phi}$$
$$+\sum_{\mathbf{k},\sigma}\epsilon_{\mathbf{k}a\sigma}a^{\dagger}_{\mathbf{k}\sigma}a_{\mathbf{k}\sigma}+\epsilon_{\mathbf{k}b\sigma}b^{\dagger}_{\mathbf{k}\sigma}b_{\mathbf{k}\sigma}+H_{\rm int}. \tag{4.1}$$

$H_{\rm int}$ is given by

$$H_{\rm int}=H_{xy}+H_{\rm anis}, \tag{4.2}$$

$$H_{xy}=\sum_{\mathbf{k},\mathbf{k}',q}\mathcal{J}_{zz}(\mathbf{k},\mathbf{k}',q)\tau_{z\mathbf{k}q}\tau_{z\mathbf{k}'\mathbf{q}}+\mathcal{J}_{\perp}(\mathbf{k},\mathbf{k}',q)$$
$$\times(\tau_{x\mathbf{k}q}\tau_{x\mathbf{k}'q}+\tau_{y\mathbf{k}q}\tau_{y\mathbf{k}'q}), \tag{4.3}$$

$$H_{\rm anis}=\sum_{\mathbf{k},\mathbf{k}',q}\mathcal{J}_{zx}(\mathbf{k},\mathbf{k}',q)\tau_{x\mathbf{k}q}\tau_{z\mathbf{k}'q}+\text{H.c.}+\mathcal{J}'_{\perp}$$
$$\times(\mathbf{k},\mathbf{k}',q)(\tau_{x\mathbf{k}q}\tau_{x\mathbf{k}'q}-\tau_{y\mathbf{k}q}\tau_{y\mathbf{k}'q}), \tag{4.4}$$

where $\tau_{\mathbf{k},q}$ are defined in a-b space [not to be confused with momentum transforms of Eqs. (3.21)–(3.23)]:

$$\tau_{z\mathbf{k}q}=a^{\dagger}_{\mathbf{k}+q}a_k-b^{\dagger}_{\mathbf{k}+q}b_{\mathbf{k}},$$
$$\tau_{x\mathbf{k}q}=\tfrac{1}{2}(a^{\dagger}_{k+q}b_{\mathbf{k}}+b^{\dagger}_{\mathbf{k}+q}a_{\mathbf{k}}), \tag{4.5}$$
$$\tau_{y\mathbf{k}q}=-\frac{i}{2}(a^{\dagger}_{\mathbf{k}+q}b_{\mathbf{k}}-b^{\dagger}_{\mathbf{k}+q}a_{\mathbf{k}}).$$

As mentioned in Sec. II, Eq. (4.1) follows directly from the ''bare Hamiltonian,'' Eq. (2.1), by transforming to the noninteracting bands using Eq. (2.5) (neglecting the terms in the first line, which only serve to renormalize parameters). The transformation from the bare U's and V's to $\mathcal{J}$s using Eq. (2.5) is straightforward and not explicitly presented here. The only important point to note is that one should always include both the particle hole channels. Thus $Vn_{di}n_{pj}$ is written as

$$\frac{V}{2}\Big[\sum_{\sigma,\sigma'}(d^{\dagger}_{i\sigma}d_{i\sigma})(p^{\dagger}_{j\sigma'}p_{j\sigma'})+(d^{\dagger}_{i\sigma}p_{j\sigma'})(p^{\dagger}_{j\sigma'}d_{i\sigma})\Big]$$
$$+\text{one-electron terms}. \tag{4.6}$$

We note that the instabilities discussed here do not occur for the model with only on-site interactions, just as in the case of the Hamiltonian derived in the strong-coupling limit. In the strong-coupling limit the kinetic energy parameters $\tilde{t}$ and Δ depend on the hole density x through the dependence of ϕ_0^2 on x derived below. This in turn makes the effective interactions $\mathcal{J}$ depend on x also. If Eq. (4.1) is considered directly derived from Eq. (2.1), the kinetic energy and the interactions are transformations of the bare terms. One can interpret the operators $a_{\mathbf{k}\sigma}$, $b_{\mathbf{k}\sigma}$ as in Eqs. (3.32) and (3.33) or as the bare band-structure operators given by Eq. (2.5).

For short-range interactions, the $\mathcal{J}$s can be written as a sum over products of separable functions with the symmetry of the lattice. In terms of the leading such terms, we define.

$$\mathcal{J}_{\eta\zeta}(\mathbf{k},\mathbf{k}',q)\equiv\sum_{s}\mathcal{J}_{\eta\zeta}\mathcal{F}^{s}_{\eta}(\mathbf{k},q)\mathcal{F}^{s}_{\zeta}(\mathbf{k}',q), \tag{4.7}$$

where $\eta,\zeta=(x,y,z)$. The form factors $\mathcal{F}_{\eta}$'s are obtained by Fourier transforming Eq. (3.26) and using the rotations (3.32) and (3.33) or directly from Eq. (2.1).

$\mathcal{F}_{\eta'}$'s have a rather messy form. I assume that there is one particular lattice harmonic which dominates and henceforth drops the superscript s. Of course, the dominant harmonic can be determined only from a detailed calculation. Such calculations are not done in this paper, nor are they necessary for the principal conclusions drawn.

In Eq. (4.1) we have dropped the mean-field decomposition (3.31). It simply renormalizes the kinetic energy in Eq. (4.1) without introducing any new qualitative features. The interaction term in Eq. (4.1) is purely in the spin-singlet channel. Due to lattice effects, couplings of the form $\tau_{y\mathbf{k}q}\tau_{z\mathbf{k}'q}$ and $\tau_{y\mathbf{k}q}\tau_{x\mathbf{k}'q}$ are also produced but they vanish as $q\to 0$ and play no essential role. I have dropped such terms.

A. Instabilities

We look for instabilities of the $q=0$ intracell excitonic nature. They can arise only if the parameters in $H_{\rm int}$ are the same scale or larger than the bandwidth. To calculate the properties of the new states, one introduces, as usual, uniform ($q=0$) mean field amplitudes, which will be determined variationally:

$$T_z\equiv\mathcal{J}_{zz}\sum_{\mathbf{k}}\langle\tau_{z\mathbf{k},0}\rangle\mathcal{F}_z(k), \tag{4.8}$$

$$T_x\equiv\frac{1}{2}\mathcal{J}_{xx}\sum_{\mathbf{k}}\langle\tau^{\dagger}_{\mathbf{k},0}+\tau^{-}_{\mathbf{k},0}\rangle\mathcal{F}_x(k), \tag{4.9}$$

$$T_y\equiv-\frac{i}{2}\mathcal{J}_{yy}\sum_{\mathbf{k}}\langle\tau^{\dagger}_{\mathbf{k},0}-\tau^{-}_{\mathbf{k},0}\rangle\mathcal{F}_y(k)\equiv\sum_{\mathbf{k}}T_y(k), \tag{4.10}$$

where $\mathcal{F}_{\alpha}(k)\equiv\mathcal{F}_{\alpha}(k,0)$. We also define the amplitude $T_{\perp}$ and angle θ by

$$T_{\perp}\equiv|T_x+iT_y|,\quad \tan\theta=T_y/T_x. \tag{4.11}$$

The splitting of the bands always provides an effective field acting on τ_z. Therefore any interesting instabilities can only be in the τ_x-τ_y plane. We therefore look for instabilities which determine the magnitude $T_{\perp}$ of an order parameter in the τ_x-τ_y plane and its angle θ, with respect to the τ_x axis.

If $H_{\rm anis}$ were ignored, the model is isotropic about the z axis. There would be just one transition of a second-order nature with massless collective fluctuations. The coupling to

fermions of the collective modes would vanish in the long-wavelength limit because these modes arise due to breaking a continuous symmetry. H_{anis} reduces the symmetry so that, as shown below, the general model has one first-order transition and two second-order transitions of the Ising variety as the parameters in the model (including μ) are varied.

Before we proceed with the calculations, it is useful to discuss the excitation spectra for interaction strength *less* than necessary to cause the instability. Consider first only H_{xy}. The problem of the excitation spectra between a partially filled band a and an empty (or fully filled) band b has been investigated in degenerate semiconductors[50] and with the approximation of a dispersionless band b for the Fermi-edge singularities[50–52] in the core spectrum of metals. The *absorption* spectrum is given by [see Fig. (9a)]

$$\chi(\omega,q)\sim\sum_{\nu}\sum_{\mathbf{k}}\Lambda(k,\nu;\omega,q)G_a(k+q,\nu+\omega)G_b(k,\nu), \tag{4.12}$$

where Λ is the complete vertex in the particle-hole channel with energy momentum (ω,q), and G_a and G_b are the (exact) single-particle Green's functions. Using the fact that band b is empty (at $T=0$), the sum over ν can be explicitly carried out with the result

$$\chi(\omega,q)\sim\sum_{\mathbf{k}}\Lambda(k,\nu;\omega,q)G_b(k,\nu)\big|_{\nu=-\omega+\epsilon_{a\mathbf{k}}-\mu}. \tag{4.13}$$

For small interactions, there is a modification of the spectra at the *threshold* energy $\epsilon_t\equiv\epsilon_b(k_F)-\mu$. We are interested only in interactions large enough that an excitonic collective mode, which does not overlap the interband a-b transitions, is pulled out. The simplest approximation for the calculations is to consider a rigid Fermi sea which only serves to block out a part of the phase space. This is the ladder diagram approximation for Λ, Fig. 9(b). In this case one obtains a sharp collective mode with spectral function $\sim\delta(\omega-\omega_{\text{ex}}(q))$. This is a poor approximation for the line shape.[51] The dressing of the exciton by low-energy particle-hole excitations at the Fermi surface—the simplest processes are represented in Fig. 9(c)—modifies the line shape nonperturbatively. The problem has been solved exactly[52] in the recoil-less limit, i.e., for a dispersionless b band where the interaction strength can be parametrized by a phase shift $\delta(\epsilon)$. In this case Λ is also independent of momentum k and χ is therefore independent of q. The absorption line shape is as sketched in Fig. 10(a). Near the excitonic threshold it is given by

$$\chi(\omega)\sim(\omega-\omega_{\text{ex}})^{-1+(1-\delta_0/\pi)^2},\quad \omega>\omega_{\text{ex}}. \tag{4.14}$$

Here δ_0 is the phase shift at the *chemical potential*, modulo π—the phase shift required to pull an exciton from the continuum. ω_{ex} is determined by the details of band structure, the density of conduction electrons, and the strength of the potential. Note that in the weak-coupling limit the absorption line shape has precisely the same exponent,[51] but the absorption edge is at the energy ϵ_t. Thus Eq. (4.14) may be regarded as the Fermi-surface singularity pulled down to ω_{ex} or that the absorption displays the excitonic edge as modified by a shakeoff of low-energy particle-hole excitations at the Fermi surface. Therefore processes which smooth the Fermi-edge singularities will also smooth the excitonic edge.

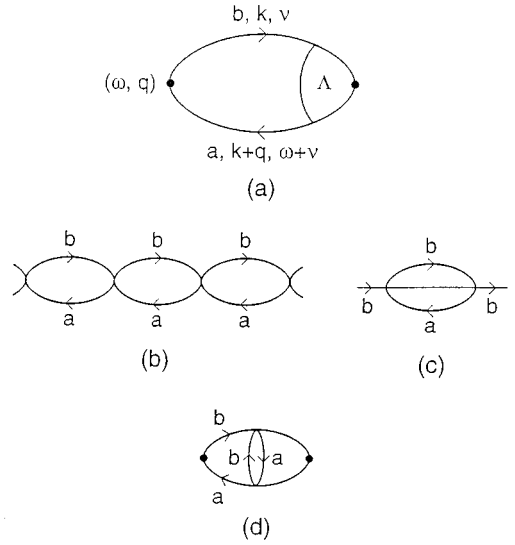

FIG. 9. Exact representation of the interband susceptibility as a function of energy ω and momentum q. The lines are exact one-particle Green's functions and Λ is the complete (reducible) vertex. (b) The interband susceptibility in the ladder diagram approximation to Λ of (a). (c) Elementary self-energy and vertex corrections neglected in (b).

The effect of a finite hole mass or recoil[50] on the Fermi-edge spectra is to smooth the singularity. Auger processes now introduce a self-energy for G_b which is smooth on the scale of the recoil energy $\epsilon_b(k_F)-\epsilon_b$ (zone boundary). All k's from the zone boundary to k_F now contribute to the absorption for any given external q, and momentum is conserved by particle-hole scattering on the Fermi surface. Both

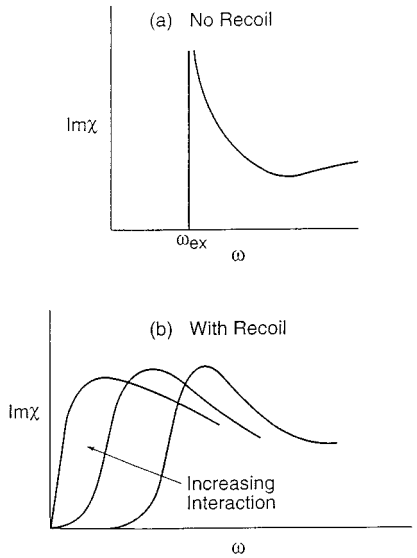

FIG. 10. (a) Interband absorption spectrum near the excitonic threshold in the approximation that band b is infinitely massive, after Ref. 52. (b) Interband absorption spectrum near the excitonic ledge with finite hole mass. The excitonic ledge shifts to lower energy as the interband interactions increase.

G_b and Λ are now functions of k. The extra integrations in Eq. (4.12) then round off the singularity over the recoil energy. If interactions are strong enough to pull out an exciton, the excitonic edge must be similarly rounded off near the excitonic edge $\omega_{\rm ex}$. This is shown in Fig. 10(b). Similar behavior must exist for a range of q from 0 to order the difference from k_F to the zone boundary. We may write qualitatively that

$$\chi(\omega,q)=\chi\left(\frac{\omega-\omega_{\rm ex}(q)}{\Gamma}\right), \tag{4.15}$$

where Γ is the smaller of the recoil energies or $\omega_{\rm ex}$. $\chi(x)$ has the form (4.14) for $x\gg 1$, but near $x=0$, $\chi(x)$ is a smooth function of x.

The two important points in the above discussion are (i) that for large enough interactions an excitonic state is pulled out with or without recoil and (ii) that recoil is always a relevant perturbation, smoothing out the singularity at the Fermi edge and therefore at the excitonic edge if it exists.

As the interaction strength in Eq. (4.1) increases, $\omega_{\rm ex}(q)$ decreases. The band structure in Eq. (4.1) is unstable for interactions for which $\mathrm{Re}\chi(0,0)\to\infty$. It appears difficult to get explicit closed form expressions for $\chi(q,\omega)$ taking into account the dressing of the exciton by low-energy particle-hole pairs. In subsequent sections, I present explicit results with the frozen Fermi-sea approximation, and then discuss from general considerations the essential features of the exact $\chi(\omega,q)$.

B. Anisotropies

The anisotropic interaction terms $\mathcal{J}_{zx}$ and $\mathcal{J}'_\perp$ play a quite different role than $\mathcal{J}_\perp$ and $\mathcal{J}_{zz}$. It is convenient to first focus on these differences. The effective interaction $\mathcal{J}_{zz}$ as derived in Appendix B is in general smaller than $\mathcal{J}_{xx}$ and $\mathcal{J}_{yy}$. But the amplitude T_z is always finite because of the splitting between the bonding-b and antibonding-a bands in Eq. (4.1), i.e., an effective uniform field $\sim\tau_z^i$. The term proportional to $\mathcal{J}_{zx}$ in Eq. (4.4) is therefore approximated as

$$\mathcal{J}_{zx}^{-1}\left[T_zT_x+T_z\sum_{\mathbf{k}}\ \tau_{x\mathbf{k}}\mathcal{F}_{xz}(k)+T_x\sum_{\mathbf{k}}\ \tau_{z\mathbf{k}}\mathcal{F}_{xz}(k)\right]. \tag{4.16}$$

T_z and T_x will therefore have no low-energy dynamics. So, at low energies, the corrections to the mean-field approximation (4.16) are unimportant. The second and third terms in Eq. (4.16) merely renormalize the band structure provided T_z and T_x are finite. The first term may be written as

$$A\cos\theta,\quad A=\mathcal{J}_{zx}^{-1}T_zT_\perp. \tag{4.17}$$

Consider next the term proportional to $\mathcal{J}'_\perp$ in Eq. (4.4). In the mean-field approximation we write it as

$$(\mathcal{J}'_\perp)^{-1}[(T_x)^2-(T_y)^2]. \tag{4.18}$$

Therefore this term acts as a quadratic anisotropy field in the x-y plane if an excitonic state condenses. This anisotropy may be written as

$$B(\cos^2\theta),\quad B=(\mathcal{J}'_\perp)^{-1}(T_\perp)^2. \tag{4.19}$$

In general, higher anisotropies are also generated from the starting Hamiltonian. I do not give their derivation but merely introduce, in the mean-field approximation, a term $C\cos^4\theta$ in the free energy. The mean-field anisotropy free energy is then

$$F_{\rm anis}=A\cos\theta+B\cos^2\theta+C\cos^4\theta. \tag{4.20}$$

A, B, and C are functions of the density of holes x as well as, in general, of temperature.

C. Condition for instability

1. Rigid Fermi sea

As already mentioned only the ladder diagrams, Fig. 8(b), are considered in this approximation.

The mean-field free energy then is

$$F_{\rm MF}=\frac{T_z^2}{4\mathcal{J}_{zz}}+\frac{T_\perp^2}{4\mathcal{J}_\perp}+(E_\phi+\lambda)\phi^2-\lambda_0 -\frac{1}{\beta}\sum_{k,m=\alpha,\beta}\ln(1-e^{-\beta(E_{km}-\mu)})+F_{\rm anis}. \tag{4.21}$$

We will be interested especially in the vicinity of the hole density where the $F_{\rm anis}$ vanishes to leading order. It is convenient then to begin the analysis by ignoring $F_{\rm anis}$. One thereby determines $T_\perp$, T_z, and ϕ. $F_{\rm anis}$ is then used to determine θ.

The variational one-electron Green's function is

$$G_0(k,\omega)=\begin{pmatrix}G_{aa}&G_{ab}\\G_{ba}&G_{bb}\end{pmatrix}=[\omega-H_0(k)]^{-1}, \tag{4.22}$$

$$H_0(k)=\begin{pmatrix}\epsilon_{ka}+\mathcal{F}_z(k)T_z&\mathcal{F}_\perp(k)T_\perp\\\mathcal{F}_\perp(k)T_\perp&\epsilon_{kb}-\mathcal{F}_z(k)T_z\end{pmatrix}. \tag{4.23}$$

The mean-field band structure $E_{k\,\alpha,\beta}$ and the eigenvectors $\alpha_{k\sigma}$, $\beta_{k\sigma}$ are obtained as usual by diagonalizing $H_0(k)$:

$$\begin{pmatrix}\alpha_{k\sigma}\\\beta_{k\sigma}\end{pmatrix}=\begin{pmatrix}c_k&s_k\\-s_k&c_k\end{pmatrix}\begin{pmatrix}a_{k\sigma}\\b_{k\sigma}\end{pmatrix}. \tag{4.24a}$$

Here

$$c_k=\cos\lambda_{k/2},s_k=\sin\lambda_{k/2},$$

$$\tan\lambda_k=\mathcal{F}_\perp(k)T_\perp/[\epsilon_{ka}-\epsilon_{kb}+2\mathcal{F}_z(k)]. \tag{4.24b}$$

Minimizing $F_{\rm MF}$ with respect to λ and μ gives

$$\phi^2+\sum_{k,m}\ f(E_{km}-\mu)=1 \tag{4.25}$$

and

$$\phi^2=x, \tag{4.26}$$

where $f(z)$ is the Fermi function. Equations (4.25) and (4.26) imply that the Luttinger theorem on the volume enclosed by the Fermi surface is satisfied.

Minimizing $F_{\rm MF}$ with respect to T_z, $T_\perp$, and ϕ yields, respectively,

$$\frac{T_z}{2\mathcal{J}_z}+\sum_{km} f(E_{km}-\mu)\frac{\partial E_{km}}{\partial T_z}=0, \tag{4.27}$$

$$\frac{T_\perp}{2\mathcal{J}_\perp}+\sum_{km} f(E_{km}-\mu)\frac{\partial E_{km}}{\partial T_\perp}=0, \tag{4.28}$$

$$2\lambda\phi+\frac{\partial E}{d\phi}+\sum_{k,m} f(E_{km}-\mu)\frac{\partial E_{km}}{\partial \phi}=0. \tag{4.29}$$

From Appendix B note that $\mathcal{J}_\perp \gg \mathcal{J}_z$. We expect T_z to have only a minor effect which is determined mainly by the ''external field'' Δ. The stability of the mean-field approximation for ϕ_i is ensured by a finite value for the ''boson'' chemical potential $E_\phi+\lambda_0$. In fact, apart from detailed quantitative issues, we need look only at Eq. (4.28) which can be rewritten as

$$\frac{1}{2\mathcal{J}_\perp}+\sum_{k,\sigma} |\mathcal{F}_\perp(k)|^2\frac{f(E_{k\alpha\sigma}-\mu)-f(E_{k\beta\sigma}-\mu)}{(E_{k\alpha\sigma}-E_{k\beta\sigma})}=0. \tag{4.30}$$

The (approximate) condition for one electron band structure to be unstable is obtained by

$$\frac{1}{2\mathcal{J}_\perp}+\sum_{k\sigma} |\mathcal{F}_\perp(k)|^2\frac{f(\epsilon_{ka\sigma}-\mu)-f(\epsilon_{kb\sigma}-\mu)}{(\epsilon_{ka\sigma}-\epsilon_{kb\sigma})}=0. \tag{4.31}$$

At $T=0$, the right-hand side of Eq. (4.31) is of order $N(0)\ln(W+\epsilon_t)/\epsilon_t$. Since the ''threshold energy'' ϵ_t and the bandwidth W are of similar order, we need $2\mathcal{J}_\perp N(0)$ of $O(1)$ to have an instability. We will in fact assume that $2\mathcal{J}_\perp N(0)$ is large enough that the instability is at a very high temperature. Stability is achieved by $T_\perp\neq 0$, which corresponds simply to changing the relative Cu and O character of the occupied and unoccupied bands. This result is no more than the statement that just as at 1/2 filling the charge state away form 1/2 filling is determined by the electron-electron interactions, not just by the one-electron band structure. This behavior has been seen in a variety of earlier calculations.[41,42] We will see below that when $F_{\rm anis}$ is considered, the transition to $T_\perp\neq 0$ becomes of first order, except at two points. It is only near those two points that interesting properties can arise.

2. Soft Fermi sea

Only the ladder diagrams are considered in the vertex Λ in deriving Eqs. (4.27)–(4.29); i.e., the Fermi sea merely acts to restrict phase space. As already discussed, this is a poor approximation. For sufficiently strong interactions the one-electron band structure is of course unstable even with the inclusion of low-energy particle-hole excitations, such as in Figs. 8(c) and 8(d). But several details change. In general, the mean-field amplitudes T_x, T_y, and T_z are functions of frequency. But as a variational ansatz, Eqs. (4.8)–(4.10) may still be introduced. The considerations of anisotropy still continue to hold as in Sec. IV B. The mean-field free energy (4.21) is an approximation of the general case, where the T and ϕ dependence (after integrating over the Fermions) may be written as

$$(T_\perp \;\; T_z \;\; \phi)\;\; \chi^{-1}\begin{pmatrix} T_\perp \\ T_z \\ \phi \end{pmatrix}. \tag{4.32}$$

Equations (4.27)–(4.29) are rigid Fermi-sea approximations of the general condition

$$\det\chi^{-1}(\omega=0,q=0)=0 \tag{4.33}$$

to determine the variational parameters $T_\perp$, T_z, and ϕ.

The qualitative form of $\chi(\omega,q)$ for an interaction strength less than the critical value has been discussed in Sec. IV A and illustrated in Fig. 10(b). Let us define p as the parameter [which is a function of the parameters in the Hamiltonian (4.1)] such that the instability towards $T_\perp\neq 0$ occurs at a temperature T_c for $p=p_c(T_c)$. First consider $T_c\approx 0$. What does the condition (4.33) for the instability imply for $\mathrm{Im}\chi(\omega,q)$ when the latter is overdamped and has the shape as in Fig. 10(b) rather than a δ-function as in the rigid Fermi-sea approximation. $\chi(\omega,q)$ has to satisfy the requirement

$$\mathrm{Im}\chi(\omega,q)=-\mathrm{Im}\chi(-\omega,q). \tag{4.34}$$

For ω small compared to $\omega_{\rm ex}$, $\mathrm{Im}\chi(\omega,0)\sim\omega$, while for ω large compared to $\omega_{\rm ex}$, it is nearly a constant up to a cutoff ω_c on the scale of the Fermi energy. Then by Kramers-Kronig transform the leading term in

$$\mathrm{Re}\chi(\omega,0)\sim\ln\left(\frac{\omega_c}{\max(\omega_{\rm ex},\omega)}\right).$$

As $p\to p_c(0)$, $\omega_{\rm ex}\to 0$. Near this point, $\mathrm{Im}\chi(\omega,0)\sim\mathrm{sgn}(\omega)$.

We see that recoil reduces the singularity as $\omega\to 0$ of $\chi(\omega,0)$ near the transition at $T=0$ as $p\to p_c(0)$ from the δ function of the rigid-sea approximation or the exact result (4.14) for the recoil-less case. In terms of Eq. (4.14) recoil makes the phase shift δ_0 at the chemical potential irrelevant. This appears quite unavoidable—on the one hand, recoil cannot prevent the instability if the interaction is large enough; on the other hand, the singularity in Eq. (4.14) which is a Fermi-edge singularity is wiped out by recoil. The result is that the instability occurs with the least singular form possible: $\chi(\omega,0)\sim\ln(\omega+i0)$. As discussed in connection with Eq. (4.15), the smoothing of the excitonic edge occurs at any external q due to the mixing by Auger processes of interband particle-hole pairs over essentially the whole range of momenta. Thus for interaction energies large compared to the Fermi energy as required for the instability and therefore also large compared to the recoil energy, the frequency dependence of the $\mathrm{Im}\chi(\omega,q)$ is nearly the same over the whole range of q. The imaginary part of $\chi(\omega,q)$ is then reminiscent of the form of the Cooper-pair-fluctuation propagator[53] above a superconductive transition which is $\sim i\omega/\max(\omega,T)$ over a range of q smaller than the coherence length ξ_0, i.e., the size of the Cooper pairs. Here, given the strong coupling required to engender the instability, the excitons have size of the order of the lattice spacing. So the $i\omega/\max(\omega,T)$ form of damping is expected to persist over most of the Brillouin zone.

The form for $\chi(\omega,q)$ near for $T=0$ as $p\to p_c(0)$ is thus

$$\chi(\omega,q)\sim\left[\left(\frac{i\omega}{\max(\omega,\omega_{\rm ex}(p))}+\ln\frac{\omega_c}{\max(\omega,\omega_{ex}(p))}\right)^{-1}+\kappa^2q^2+[p_c(0)-p]\right]^{-1}, \tag{4.35}$$

where ω_c is an upper cutoff energy, and κ provides the scale of dispersion. At a finite temperature, we must use the fact that the ω and T dependence in $\chi(\omega,q)$ must scale as ω/T. So, for $T\gg\omega$,

$$\chi(\omega,q,T)\sim\left[\left(\frac{i\omega}{\max(T,\omega_{\rm ex}(p))}+\ln\frac{\omega_c}{\max(T,\omega_{\rm ex}(p))}\right)^{-1}+\kappa^2q^2+[p_c(T)-p]\right]^{-1}. \tag{4.36}$$

D. Determining θ

We now consider the effects of $F_{\rm anis}$. On minimizing $F_{\rm anis}$ with respect to θ, one finds that the equilibrium value Θ_m is given by

$$\Theta_m=0 \quad \text{for } (A+2B+4C)<0 \tag{4.37}$$

for phase I and

$$\Theta_m=\pi \quad \text{for } (-A+2B+4C)<0 \tag{4.38}$$

for phase I′.

For $C>0$, there occurs a second order transition of the Ising variety to

$$0<\Theta_m<\pi \quad \text{for } -A<2B+4C<A \tag{4.39}$$

for phase II. Θ continuously rotates in phase II as A,B,C vary.

Noting that A,B,C are in general functions of x and T, we may write the mean-field anisotropy energy as

$$F_{\rm anis}=G_0(x,T)[\theta-\Theta_m(x,t)]^2+\cdots, \tag{4.40}$$

where

$$G_0(x,T)=0 \quad \text{for } \pm A+2B+4C=0, \quad \text{i.e., } \Theta_m=0,\pi. \tag{4.41}$$

Therefore the transition at $\Theta_m=0$ or π is of second order. Let us denote the transition line (understanding that as x is varied we will be concerned only with either I to II or I′ to II transition) by $x_c(T_c)$.

Let us stay for definiteness in the vicinity of $\Theta_m=0$. For $\Theta_m=0$, the high-temperature transition occurs as a first-order transition with a real order parameter T_x. When $\Theta_m\neq0$, the mean-field order parameter is complex: T_x+iT_y. $T_y\neq0$ implies that in the ground state, a current distribution occurs within each unit cell which has the same phase in every unit cell.

The content of the mean-field theory is summarized in Fig. 5, where the free energy is shown as a function of T_x and T_y and in Fig. 8. Throughout the temperature region of interest $T_x\neq0$. As $(p\equiv\pm A+2B+4C)$ is varied by varying x (and T), a second-order Ising transition from $T_y=0$ to the circulating current phase $T_y\neq0$ occurs. (We note in passing that we have arrived at a new class of statistical-mechanical model for quantum-critical points.)

We will discuss below how regimes 1 and 3 of the phase diagram of Fig. 1 may be identified with the phase I (or I′) and regimes 2 and 4 with the phase II of the mean-field theory. The nature of the fluctuations will be shown to vary in phase I as a function of x and T leading to a crossover in the properties from regime 1 to regime 3 in Fig. 1. We will also show that the phase transitions between phase I and phase II also becomes a crossover for arbitrarily small disorder.

E. Circulating current phase

$\Theta_m\neq(0,\pi)$ implies that in the ground state, a current flows in each cell. Since the momentum of the instability is zero, the current pattern respects lattice-translation symmetry. The current pattern within a cell can be deduced from the mean-field Hamiltonian with $\Theta\neq0$, which is now Eq. (4.23) with the substitution $T_\perp\to T_\perp e^{i\Theta}, T_\perp e^{-i\Theta}$ in the off-diagonal terms. To calculate the current pattern, first find the eigenvectors of the conduction band with $\Theta\neq0$:

$$E_\alpha(k)\hat\alpha_{k\sigma}=[\epsilon_{ka}+\mathcal{F}_z(k)T_z]a_{k\sigma}+\mathcal{F}_\perp(k)T_\perp e^{i\Theta}b_{k\sigma}. \tag{4.42}$$

Now use Eqs. (2.5) to express a,b in terms of d_k and $p_{x,y}(k)$ using coefficients given in Appendix A. This yields

$$\hat\alpha_{k\sigma}=\hat u_{\alpha d}(\mathbf{k})d_{\mathbf{k}\sigma}+\hat u_{\alpha x}(\mathbf{k})p_{x\mathbf{k}\sigma}+\hat u_{\alpha y}(\mathbf{k})p_{y\mathbf{k}\sigma}, \tag{4.43}$$

where $\hat u$'s are complex coefficients:

$$\hat u_{\alpha(d,x,y)}(k)\equiv R_{\alpha(d,x,y)}(k)e^{i\phi_{(d,x,y)}(k)}. \tag{4.44}$$

There is no need to exhibit the complicated expressions for these coefficients because the current pattern can be deduced from their general properties specified below.

The current in a bond going from a copper site to an oxygen site in the x or y direction is

$$j_{dx}=\frac{2}{\pi}t_{pd}\,\mathrm{Im}\langle d^\dagger_{i\sigma}p_{i+x,\sigma}\rangle=\frac{2a}{\pi}\,t_{pd}\sum_{k<k_F}\cos\frac{k_xa}{2}R_{\hat\alpha d}R_{\hat\alpha x}\sin[\phi_d(k)-\phi_x(k)]. \tag{4.45}$$

[The sum over k of the term with $\sin(k_xa/2)$ is zero using inversion symmetry.] Now note that t_{pd} changes sign $x\to-x$ and the sum in Eq. (4.45) is symmetric under inversion. Hence the current between a copper orbital at a site i and an oxygen orbitals at $i+(a/2)\hat x$ and $i-(a/2)\hat x$ are equal and opposite. This holds also for the current between copper orbitals at i and oxygen orbitals at $i\pm(a/2)\hat y$.

The current between two oxygen orbitals in the same cell,

$$j_{xy}=\frac{at_{pp}}{a}\mathrm{Im}\langle p^{\dagger}_{i+x,\sigma}p_{i+y,\sigma}\rangle$$

$$=\frac{2at_{pp}}{a}\sum_{\mathbf{k}<k_F}\cos\frac{k_{xa}-k_{ya}}{2}\;R_{\hat{\alpha}x}(\mathbf{k})R_{\hat{\alpha}y}(\mathbf{k})$$

$$\times\sin[\phi_x(\mathbf{k})-\phi_y(\mathbf{k})]. \tag{4.46}$$

The sum in Eq. (4.46) is identical for the other three oxygen-oxygen bonds around a given copper atom, but as is evident from the phases shown in Fig. 8. t_{pp} reverses sign cyclically in going around the four bonds, and therefore so does the current.

The direction of the current between the copper and the oxygen orbitals and between the oxygen orbitals fixes the pattern show in Fig. 6. So, together with breaking time-reversal symmetry, fourfold rotational symmetry is broken. But the product of the two is left invariant.

Some further conclusions can be drawn from an examination of the $\hat{u}$'s. If $t_{pp}=0$, $\psi_{\alpha x}(\mathbf{k})=\psi_{\alpha y}(\mathbf{k})$. Then any $[\psi_{\alpha d}(k)-\psi_{\alpha x,y}(k)]$ can be removed by a unitary transformation without affecting the eigenvalues or the eigenvectors. This is physically obvious from looking at Fig. 6; a current between copper and oxygen orbitals is meaningless in the absence of a current between the oxygen orbitals.

We can also deduce that there is no contribution to the currents from states on the diagonals in the Brillouin zone, $\pm k_x=\pm k_y$. Correspondingly, there is no change in the single-particle eigenvalues in the circulating current phase along the diagonals. On zone faces $k_x=0$ or π/a, $k_y=0$ or π/a, the eigenvalues do change. The lowest lattice harmonic consistent with these symmetries is $d_{x^2-y^2}$. So there is a change in the single-particle spectra in the circulating current phase of $d_{x^2-y^2}$ symmetry.

The ground-state current contribution of each state $\mathbf{k}$ depends on $\mathbf{k}$ and there is $O(1)$ electron per unit cell in the conduction band. The orbital magnetic moment of the circulating current in each of the quadrants in Fig. 6 is $O(0.05\mu_B)$, with the assumption that the average state contributes $\sim 1/4\mu_B$ per unit cell.

V. COLLECTIVE MODES AND FERMION-BOSON COUPLING

We now consider the fluctuations in the state $T_{\perp}\neq 0$. They are interesting only near the I (or I′) to II transition. There is always a finite effective field coupling linearly to T_z. So the fluctuations in the z direction are always massive. The interesting modes are in the T_x-T_y space. So define

$$\delta T_{x,q}=\frac{1}{2}\mathcal{J}_{xx}\sum_k\langle\tau^{+}_{k,q}+\tau^{-}_{k,q}\rangle\mathcal{F}_x(k,q)-T_x, \tag{5.1}$$

$$\delta T_{y,q}=-\frac{i}{2}\mathcal{J}_{yy}\sum_k\langle\tau^{+}_{k,q}-\tau^{-}_{k,q}\rangle\mathcal{F}_y(k,q)-T_y. \tag{5.2}$$

The effective Hamiltonian determining the fluctuations is

$$H_{\mathrm{fluc}}=\sum_{k\sigma}(a^{\dagger}_{k\sigma}b^{\dagger}_{k\sigma})H_0(k)\begin{pmatrix}a_{k\sigma}\\ b_{k\sigma}\end{pmatrix}+\sum_q\frac{1}{4\mathcal{J}_{\perp}}(\delta T^{\dagger}_{x,q}\delta T_{x,q}+\delta T^{\dagger}_{y,q}\delta T_{y,q})+\sum_{k,q}\mathcal{F}_{\perp}(kq)(a^{\dagger}_{k+q}b_k+b^{\dagger}_{k+q}a_k)(\delta T_{x,q}+\delta T^{\dagger}_{x-q})$$

$$+i\sum_{k,q}\mathcal{F}_{\perp}(kq)(a^{\dagger}_{k+q}b_k-b^{\dagger}_{k+q}a_k)(\delta T_{y,q}+\delta T^{\dagger}_{y,-q})+H_{\mathrm{anis}}. \tag{5.3}$$

Again, let us ignore the effects of anisotropy to begin with but choose $\Theta_m=0$, i.e., $T_{\perp}=T_x$. The spectrum of the fluctuations

$$D^0_x(q,\omega)\equiv\langle\delta T_x\delta T_x\rangle(q,\omega), \tag{5.4}$$

$$D^0_y(q,\omega)\equiv\langle\delta T_y\delta T_y\rangle(q,\omega) \tag{5.5}$$

is given in the frozen Fermi-sea approximation [Fig. 8(b)] by

$$\begin{Bmatrix}D^{0\,-1}_x(q,\omega)\\ D^{0\,-1}_y(q,\omega)\end{Bmatrix}=\frac{1}{2\mathcal{J}_{\perp}}+\sum_{k,\nu}|\mathcal{F}(k,q)|^2$$

$$\times[G_{aa}(k+q,\omega+\nu)G_{bb}(k,\nu)$$

$$\pm G_{ab}(k+q,\omega+\nu)G_{ba}(k,\nu)]. \tag{5.6}$$

At $\omega=0$, $q\to 0$, the equation for D^0_y is identical to Eq. (4.30) determining T_x. So a long-wavelength massless phase or current mode exists as is to be expected when the anisotropy in the τ_x-τ_y plane is zero. The poles of D^0_x give the dispersion of the amplitude modes. Their frequencies near $q\approx 0$ are of order T_x; they will not be considered further.

Let us now include the effect of anisotropy, but stay near I to II (or I′ to II) instability. From Eq. (4.40), the anisotropy energy provides a quadratic term $G_0(x,T)\,\delta T^2_y$ to the fluctuations. Including this effect

$$D^0_y(\mathbf{q},\omega)=\frac{m/m^*}{\omega^2-\kappa^2q^2+G_0(x,T)}, \tag{5.7}$$

where κ/a is the order of T_x. The spectral weight of the collective mode m^*/m is

$$\frac{m^*}{m}\sim 0(T_x/W). \tag{5.8}$$

Equations (5.6) are special cases, in the rigid Fermi-sea approximation of the general equation

$$\chi^{-1}(q,\omega)=0, \tag{5.9}$$

which determines the fluctuation spectra, just as Eqs. (4.27)–(4.29) are special cases of Eq. (4.33) which determines the one-particle spectra through fixing T_x, etc. In the frozen Fermi-sea approximation, there is no damping of the collective fluctuations—the excitonic resonances have a spectral function proportional to a δ function. As discussed in Sec. IV A for the case when $T_x=0$, inclusion of low-energy particle-hole fluctuations changes the spectral function of the excitonic collective mode in an essential way. The $\chi(q,\omega)$ including low-energy particle-hole fluctuations with $T_x\neq 0$ has the same functional form as discussed in Sec. IV C, but calculated with the new band structure, Equations (4.23) and (4.24). The dispersion of the soft excitonic collective mode at $q\rightarrow 0$, described by $D_y^0(q,\omega)$, again has the same form for $G=0$ as discussed in Sec. IV C, leading to Eqs. (4.35) and (4.36). Including the effect of the anisotropy on the fluctuations, we have

$$D_y^0(q,\omega)=D_0\left[\left\{\frac{i\omega}{\max(|\omega|,T,G_0)}+\ln\left(\frac{\omega_c}{\max(|\omega|,T,G_0)}\right)\right\}^{-1}+\kappa^2q^2+G_0(x,T)\right]^{-1}. \tag{5.10}$$

Here D_0 parametrizes the spectral weight of the fluctuation expected to be of $O(E_F^{-1})$. The second-order transition occurs when $G_0(x,T)=0$ as in Eqs. (4.37)–(4.39). (Henceforth G_0 is dimensionless, having been scaled by D_0^{-1}.) The fluctuations have a finite frequency G_0 above and a finite value below the transition (characteristic of transitions of the Ising class).

Equation (5.10) is crucial in the analysis below of the properties of the model. It is clear that the very singular result from the rigid Fermi-sea approximation, Eq. (5.7), is quite incorrect. (It also gives properties in $d=2$ which are too singular compared to experiment.) The combined effect of infrared processes at the Fermi surface and recoil together with analyticity requirements has been discussed in Sec. IV C to lead to Eq. (5.10). This justification is only heuristic. An evaluation of processes like in Fig. 9(c) to find Λ exactly appears very hard, if not impossible. Earlier, a three-body scattering approach to the problem was suggested.[54] It might be possible to evaluate $D_y(q,\omega)$ systematically in such an approximation. Note that when δ_0 of Eq. (4.14) is zero, as argued here, $\mathrm{Im}G_b(\omega)\sim\omega^{-1}$, at least for the recoilless case.[50] This is consistent with the conjecture[54] that a three-body resonance at the chemical potential may lead to the observed normal-state anomalies.

There are no other massless modes in the model. Earlier investigations[41,42] of the charge-transfer instability in the model found a diverging compressibility indicating phase separation. If one adopts a short-range interaction model, the density fluctuations have a dispersion $\omega\sim q$. Near the critical point of the charge-transfer instability, a low-energy mode of δT_x couples to such density fluctuations pushing the ''electron sound velocity'' to zero. In a model with Coulomb interactions, the density fluctuations are at the plasma frequency. Phase separation then does not occur [unless the system has inhomogeneously distributed fixed (ionic) charges].

Consider now the coupling of the fermions to the low-energy collective modes in the vicinity of $x_c(0)$ where a transition from $T_\perp=T_x$ to a *complex* order parameter T_x+iT_y occurs. The coupling of the Fermions to the δT_y fluctuations comes from the fourth term in Eq. (5.3) and a similar term in Eq. (4.4). We must reexpress the fermion operators in terms of the low-energy fermions created by $\alpha_{k\sigma}^\dagger$ by using the rotation (4.24). The coupling is written as

$$H_{F\text{-}B}=\sum_{k,q,\sigma} i\ \ g(k,q)\ \ \alpha_{k+q,\sigma}^\dagger\alpha_{k,\sigma}(\delta T_{yq}+\delta T_{y-q}^\dagger). \tag{5.11}$$

One finds from the fourth term in Eq. (5.3) [the corresponding term from Eq. (4.4) introduces no important difference]

$$g(k,q)=g_0\ \ \mathcal{F}_y(k,q)\sin\left(\frac{\lambda_{k+q}-\lambda_k}{2}\right). \tag{5.12}$$

In Eq. (5.12) we have introduced g_0 with dimensions of energy, so that δT_y is henceforth dimensionless. g_0 is expected to be of $O(E_F)$. In general $\mathcal{F}_y(k,q)$ is finite for $q\rightarrow 0$, but $g(k,q)$ vanishes linearly with q. So, even through we have an Ising transition, the coupling of the Fermion to the fluctuations vanishes at long wavelength. This occurs because the bands are split due to ''external'' fields and the fact that no $\tau_x\tau_y$ or $\tau_z\tau_y$ coupling is allowed at long wavelengths. The vanishing of the coupling at long wavelengths is, however, not fatal because in the fluctuation spectrum, Eq. (5.10), all q's are (to a logarithmic accuracy) equally important in properties which integrate the spectrum to energies of the order of temperature.

VI. ANALYSIS OF THE LOW-ENERGY HAMILTONIAN

The end result of the preceding two sections is a simple Hamiltonian for the calculation of low-energy properties:

$$H=\sum_{k,\sigma}\epsilon(k)\alpha_{k\sigma}^\dagger\alpha_{k\sigma}+D_y^{0\,-1}(q,\omega)\delta T_{y,q}^\dagger\delta T_{y,q}+\sum_{k,q} ig(k,q)\alpha_{k+q\sigma}^\dagger\alpha_{k,\sigma}(\delta T_{y,q}+\delta T_{y,-q}^\dagger). \tag{6.1}$$

We now analyze the properties of this Hamiltonian in the regime near the I to II transition near $T=0$.

It is best to start by considering the simple physical processes depicted in Figs. 11(a)–11(f). Here the wiggly lines denote the fluctuation propagation $D_y^0(q,\omega)$ and the solid lines the fermion propagation $G_0(k,\omega)=\langle\alpha\alpha^\dagger\rangle(k,\omega)$.

The real part of Fig. 11(a) for $q\rightarrow 0$, $\omega\rightarrow 0$ renormalizes the mass G. This can be absorbed in a redefinition of x_c. Similarly the leading q dependence $\sim q^2$ merely redefines the coefficient κ in Eq. (5.10). The imaginary part gives the usual Landau damping contribution $\sim\ i\omega/v_Fq$. If we use renormalized fermion propagators in Fig. 11(a), the result is modified to

$$i\omega/\max(\mathrm{Im}\Sigma(\omega,T,G),v_Fq).$$

We will show that in the non-Fermi-liquid regime $\mathrm{Im}\Sigma(\omega,T)\sim\max(\omega,T)$. This is an additive correction to the imaginary part in Eq. (5.10) and is therefore unimportant at

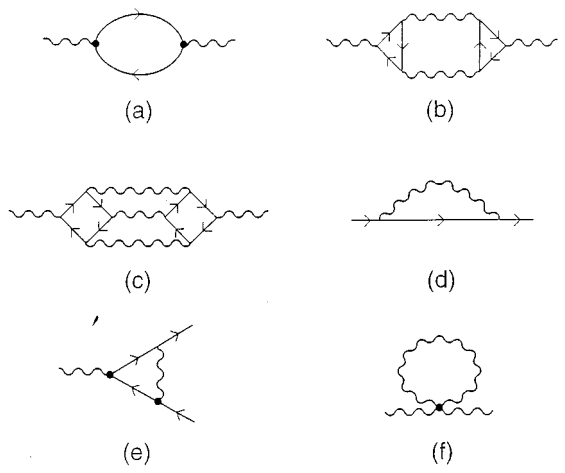

FIG. 11. Processes for analysis of the low-energy Hamiltonian; (a), (b), (c) are processes considered for the boson self-energy, (d) for the fermion self-energy. (e) is the lowest-order correction to the boson-fermion vertex. (f) Leading self-energy due to anharmonic interaction between the fluctuations.

all q. This would not be true in the rigid Fermi-sea approximation in which the fluctuations in $D^0(q,\omega)$ are completely undamped. (In that case D^0 has the same functional dependence on q and ω as the transverse electromagnetic field propagators in a metal[55].) One can also examine higher-order renormalizations, Fig. (11b) and Fig. (11c) to conclude that they are irrelevant, and the imaginary part of the process in Fig. 11(b) is proportional to ω while Fig. 10(c) is proportional to ω^2.

Consider next the fermion self-energy graph, Fig. 11(d). The imaginary part of the self-energy is easily seen to be

$$\mathrm{Im}\Sigma(q,\omega)=N(0)\int_0^1 d^{d-1}x\int_{\epsilon_1}^{\epsilon_2}d\epsilon\,\mathrm{Im}D_R^0(2k_Fx,\omega-\epsilon)\times g^2(2k_Fx)\left[\tanh\frac{\epsilon}{2T}+\coth\frac{\omega-\epsilon}{2T}\right], \tag{6.2}$$

where

$$\epsilon_{1,2}=v_F(|q|\mp k_Fx)+\mathrm{Re}\Sigma(\epsilon_{1,2}). \tag{6.3}$$

It is found consistent to ignore $\Sigma(\epsilon)$ in the right-hand side of Eq. (6.3). For $T=0$, the limits of ϵ integration are 0 to ω [except for an ignorable region of x integration of $0(\omega/E_F)$]. The x integration, using Eq. (5.10) for D_0 for $G_0=0$, then leads to a constant, so that the final result is proportional to $\omega\mathrm{sgn}\omega$. Similarly for $T\ll\omega$, the result is proportional to $T\mathrm{sgn}\omega$. The self-energy has negligible momentum dependence (if the Fermi surface has no significant nesting). These results are true for any dimension more than 1. The d independence of the self-energy, and other properties in which these fluctuations are sampled over energies to the scale of the external frequency and temperature, arises because in Eq. (5.10) the fluctuations are essentially local [even though $\mathrm{Re}D(0,0)$ diverges as G^{-1}]. We may express both the real part and the imaginary part of the self-energy by an expression which interpolates between the $\omega/T\ll1$ and the $\omega/T\gg1$ limits:

$$\Sigma(\omega,T)=\pi\lambda\left[(2\omega/\pi)\ln\left(\frac{\pi T+i\omega}{\omega_c}\right)+i\pi T\right]. \tag{6.4}$$

Equation (6.4) may be useful in analyzing angle-resolved photoemission experiments discussed below.

Consider next the vertex correction shown in the graph of Fig. 10(e). In the limit $q\to0$ first and then $\omega\to0$, it is given by a Ward identity (in the pure limit),

$$\Lambda^{\omega}=\frac{1}{z}, \tag{6.5}$$

where z is the quasiparticle renormalization amplitude given by Eq. (1.2). In the ''q limit'' it is given by another Ward identity in terms of $d\Sigma/\partial k$. Since Σ is found very weakly dependent on $(k-k_F)$, this is ignorable.

For general ω and q, a finite vertex correction $O(g)$ nonsingular as a function of ω and $k-k_F)$ is found. If the ''bare'' coupling constant $g(k,q)$ is less than $O(1)$, this may be simply absorbed in the redefinition of $g(k,q)$. One can formally devise $1/N$ schemes to keep such vertex corrections controlled.

We briefly consider the renormalization of G_0 in $D_0(q,\omega)$ due to anharmonic interactions. The leading contribution comes from

$$u|\delta T_{q,\omega}|^2|\delta T_{q'},\omega'|^2, \tag{6.6}$$

where $u>0$ is a phenomenological coefficient expected to be on the same scale as the upper cutoff energy of the fluctuations. The self-energy of the modes proportional to u, Fig. 11(f), has the leading temperature correction proportion to uT (independent of d) for $x\approx x_c(0)$. This may be absorbed in $x_c(T)$ and suppresses the transition temperature. (Henceforth we can drop the superscript 0 on G and D.) A proper analysis of the fluctuations near the transition line which changes from a quantum transition at $T=0$ to a classical Ising transition at high temperature has not been carried out.

A very important general point to note in this connection is that the correlation length exponent ν at $T=0$ as a function of $(x-x_c)$ is 0 while it is 1 for the $d=2$ classical Ising model. This is expected to turn the transition line to a crossover for arbitrarily small disorder as discussed in Sec. VIII.

We can estimate roughly the different regimes of fluctuations from the properties of the propagator $D(q,\omega)$. No sophisticated analysis of the crossover between different regimes is attempted. Consider first the departure of the transition temperature of the circulating current phase from $T=0$ at $x=x_c(0)$. We assume parameters are such that at $T=0$, the CC phase occurs for $x\leqslant x_c(0)$. This guess is based on the parameters calculated in Appendix B and the decrease of Δ with x and can be checked only through a detailed evaluation of Eqs. (4.27)–(4.29). Then the transition temperature $T_c(x)$, given by the divergence in $\mathrm{Re}D(0,0)$, is at

$$\left(\ln\left|\frac{\omega_c}{\max(T_c,G)}\right|\right)^{-1}=-G\quad\text{for}\quad G<0. \tag{6.7}$$

This gives

$$T_c\simeq-G(T_c); \tag{6.8}$$

i.e., the transition temperature is essentially proportional to $-G(0)$.

For finite $T_c(G)$, in a narrow temperature ΔT_c region near $T_c(G)$, the fluctuations are characteristic of the classical Ising model. We have not investigated here how the width of this regime varies with T_c. In this regime, the classical thermal occupation of fluctuations (where $\frac{1}{2}\coth(\omega/2T) = [n(\omega/T)+\frac{1}{2}] \approx T/\omega$) determines the thermodynamic and other properties because the characteristic energy of the fluctuations is $O(\Delta T_c) \ll T$. If the characteristic energy of the fluctuations is much larger than T, the zero-point occupation of the fluctuations dominates the properties (in this regime $\coth\omega/T \approx 1$). The physical properties in this regime are governed by the quantum fluctuations. Within this regime, we must distinguish when the characteristic scale of the fluctuations is given by temperature itself and when it is given by $G(x)$. The former is the non-Fermi-liquid regime and the latter the Fermi-liquid regime. From the form of $D(q,\omega)$, the crossover between the two occurs at $T \approx G(x)$ for $G>0$.

The momentum-integrated fluctuation spectrum for $T \gg |G|$ gives a measure of the frequency distribution:

$$\int d^2q \,\mathrm{Im}D(q,\omega)$$

$$\approx \frac{1}{\pi}\left\{\pi/2 - \tan^{-1}\left[\frac{\max(\omega,T)}{\omega}\left(\ln\frac{\omega_c}{\max(\omega,T)}\right)^{-1}\right]\right\}$$

$$\sim \frac{\omega}{T}\ln\frac{\omega_c}{T} \quad (\text{for } \omega \ll T)$$

$$\sim \ln\frac{\omega_c}{\omega} \quad (\text{for } \omega \gg T). \tag{6.9}$$

Above the narrow critical regime near $T_c(G)$, the properties are governed by the quantum fluctuations. Non-Fermi-liquid behavior is to be expected. For $G<0$, i.e., the ordered side, the fluctuations have a gap. So Fermi-liquid behavior (but with unusually small parameters) is to be expected in the pure limit. We have not yet calculated the change in one-particle spectra due to the change in dispersion in this region discussed in Sec. IV E and the change in the spectral function due to the altered fluctuations.

For $G>0$, the fluctuations have a gap of $O(G)$ for $T \ll G$. Fermi-liquid behavior is therefore to be expected but with parameters determined by G.

The different regimes are shown in Fig. 12. We are now ready to calculate the physical properties of Eq. (6.1). Given Eq. (6.1), all physical properties can be calculated in a controlled and systematic fashion because of the unimportance of vertex corrections in the fermion-boson scattering and the boson propagator. For instance, the single-particle self-energy may be calculated self-consistently by using the renormalized Fermion propagator in Fig. 11(a). The answer remains unaltered as in other problems with momentum-independent self-energy. In the fluctuation spectra (5.10), all momenta are equally important to logarithmic accuracy in the regime controlled by the quantum-critical point: q scales as $\ln\omega$. Formally this corresponds to a dynamical critical exponent $z_d \to \infty$. This appears crucial to understanding many of the observed anomalies in copper-oxide metals. It should be noted that the propagator (5.10) for $G=0$ is not the $z_d=\infty$ limit of the propagators discussed for example in Ref. 13, which are $\sim(i\omega/q^\beta+q^\alpha)^{-1}$, with z_d defined to be $(\alpha+\beta)$.

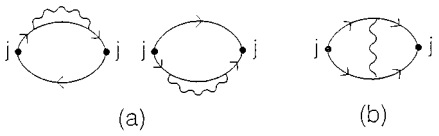

FIG. 12. Elementary processes for optical conductivity.

VII. PHYSICAL PROPERTIES

The transport properties in regime I (see Fig. 8) which are controlled by the quantum-critical point and the crossover to the customary behavior at low temperature for the overdoped case, region III, are calculated below.

In the pure limit, region II should show Fermi-liquid properties but with different parameters from region III due to the alteration of states near the Fermi surface by $T_y \neq 0$. In the next section I argue that the transition between region I and II is only a crossover and that at low temperatures region II is dominated by disorder such that the density of states at the chemical potential is zero. One should, however, expect a bump in C_v/T and χ at the I to II crossover. There is a decrease in low-energy fluctuations in region II as G_0 in Eq. (5.10) is finite. But with the density of states at the chemical potential tending to zero at low temperatures due to disorder, a Fermi-liquid behavior may never be observable except in very pure samples.

In the pure limit, although an order parameter develops in region II, it is by no means clear that there exist observable singularities in C_v/T or χ at the transition. Certainly, at $\nu=0$, $z=\infty$, no singularities exist. The crossover to Ising singularities (only logarithmic in the specific heat) at high temperatures for x far from x_c may occur with a very small amplitude at observable temperatures. This requires further work.

A. Single-particle spectra: Angle-resolved photoemission experiments and single-particle tunneling

A one-particle self-energy of the form (1.1) was suggested on phenomenological grounds.[12] While angle-resolved photoemission spectroscopy (ARPES) experiments were soon found consistent[15] with this behavior, there has been since then a considerable development in such experiments. Closer bounds should be put to this prediction. A useful formula to fit the self-energy which interpolates properly between $\omega/T \ll 1$ and $\omega/T \gg 1$, while obeying analyticity requirements, is given by Eq. (6.4). At low energies and low temperatures this behavior is modified in an interesting way by defects, as discussed later.

Single-particle tunneling has traditionally been a powerful tool for measuring the frequency dependence of the single-particle spectra. Here, the interpretation of the tunneling spectra is complicated by the fact that if the self-energy is momentum independent, its effect is not felt in the tunneling spectra unless the tunneling matrix element is momentum dependent. The situation has been amply discussed in Ref.

14 and need not be repeated. Under suitable conditions, the conductance as a function of voltage, $G(V)-G(0) \sim \mathrm{Im}\Sigma(V) \sim V$, as observed for tunneling in the c direction. The observed $G(V)$ varies weakly for tunneling in the a-b plane. This has also been discussed. A new experimental development is the observation[56] by inelastic scanning tunneling microscopy that $[G(V)-G(0)]/|V|$ increases as the distance of the tip to the surface increases thereby decreasing $G(0)$. This is in accordance with Ref. 14.

As in the case of superconductivity through electron-phonon scattering, tunneling spectroscopy should serve to identify the spectra of the glue for superconductivity.[57] If the collective mode $D(q,\omega)$ is the glue, the tunneling conductance in the superconducting state, $G(V)-G(0) \sim |V|$, above the superconducting gap as observed in appropriate geometry. Quantitative verification of these ideas has been difficult because the slope of the conductance curve depends on ''extraneous'' factors as discussed. But it should be possible in carefully designed experiments to normalize away the extraneous factors. After normalization the slope should depend only on the coupling constant which determines the superconducting transition temperature T_c.

B. Long-wavelength transport properties

As discussed in Sec. I, an important constraint is put on a theory of copper-oxide metals by the fact that if the long-wavelength transport properties are interpreted by kinetic theory or by semiclassical Boltzmann equations, the scattering rate for momentum loss measured in electrical resistivity and the scattering rate for energy loss measured in thermal conductivity have the same temperature dependence. Within experimental uncertainty, the single-particle scattering rate measured in tunneling or ARPES experiments also has the same frequency dependence. This is especially surprising in a theory in which the breakdown of Fermi-liquid theory is sought through a critical point where the long-wavelength susceptibility diverges. One might imagine then that only long wavelength fluctuations or forward scatterings are important in scattering the fermions, so that the backward scattering required in momentum transport would make the transport rate for momentum have a higher temperature dependence than in the energy transport.

The backward scattering is enforced in momentum transport usually through considering the two processes shown in Fig. 12. If, for instance, the bosons are acoustic phonons, the leading T^3 contributions to the dc resistivity of each of the processes in Fig. 13 is exactly cancelled leading to a resistivity proportional to T^5.

The situation is quite different with $D(q,\omega)$ of the form (5.10). Then there is no cancellation to leading order between the self-energy and the vertex diagrams of Fig. 12 because for energy transfer of the order temperature, momentum transfer throughout the zone is important. If $D(q,\omega)$ were truly independent of momentum, as assumed in the marginal Fermi-liquid phenomenology,[12] Fig. 12(b) would be identically zero due to the vector nature of the incoming and outgoing vertices. This is generally true for any ''s-wave'' scattering. With $D(q,\omega)$ of the form (5.10), the s-wave scattering part for $\omega \approx T$ and k and k' both on the Fermi surface

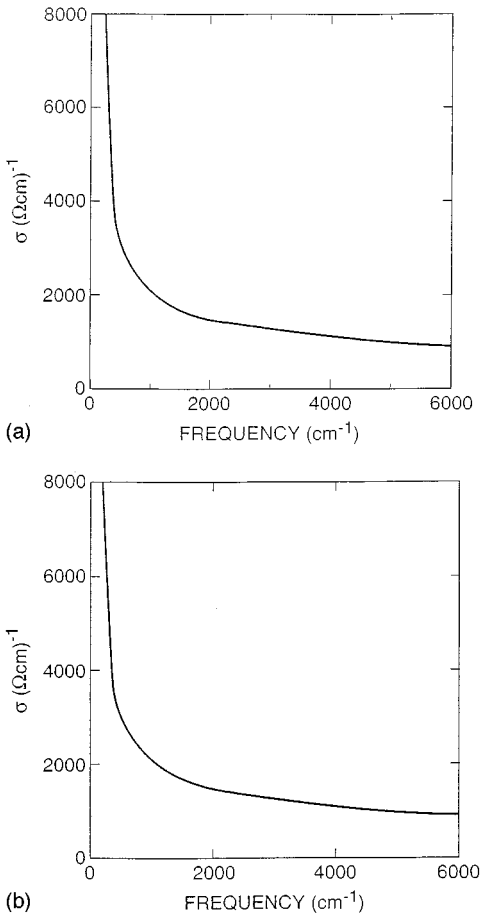

FIG. 13. (a) The calculated optical conductivity based on the theory which reproduces results based on phenomenology in Refs. 12(a) and 12(b). The parameters used are $\omega_p \approx 2$ eV, $\lambda = 0.5$, and $\omega_c = 1200$ K. A soft cutoff is used. (b) Experimental results for the optical conductibility in the basal plane, from Ref. 60.

$$\sim \frac{1}{2\pi}\int_0^{2\pi} d\theta \frac{\sin^4\theta}{1+\sin^4\theta} \tag{7.1}$$

is $O(1)$. One can show by an explicit calculation that the part of the process of Fig. 12(b) for $\omega \ll T$ does not change the argument. The conductivity can therefore be calculated from Figs. 12(a) alone with just a numerical renormalization of the coefficient. Note that due to lattice effects, conservation of momentum with initial and final states on the Fermi surface does not imply conservation of current. If for arbitrarily small ω scattering occurs from a given state on the Fermi surface to a substantial part of the Fermi surface, resistivity limited only by the density of fluctuation results. Since the *density of states* of the fluctuations is essentially a constant, a linear-in-T resistivity is to be expected.

The calculation of electrical resistivity, optical conductivity, thermal conductivity, and Raman scattering intensity from Eq. (6.1) is therefore essentially the same as done earlier,[12(a),12(b)] with similar results apart from logarithmic corrections.

1. Optical conductivity

Optical conductivity as a function of ω and T is a much more stringent test of the theory than $\rho(T)$ alone. The con-

ductivity at near-ideal doping has a very slow high-frequency falloff unlike the ω^{-2} Drude form. When vertex corrections are unimportant, as in the present theory, the conductivity can be calculated from the single-particle Green's function alone. Then the conductivity at frequencies up to $O(\omega^c_{-1})$ is $\sim[\mathrm{Im}\Sigma(\omega)]^{-1}$ with logarithmic correction. Detailed comparisons with experiments have recently been done by Abrahams.[58] Earlier calculations were reported in Ref. 12(b). For completeness and to show the quality of the fit to the experiments, the experimental results for the in-plane conductivity deduced for untwinned single crystal is shown on the same scale with the calculations with indicated parameters in Figs. 13(a) and 13(b), respectively.

The microscopic theory from the strong-coupling limit, Sec. III, provides an additional important feature: The (intraband) optical conductivity sum rule is

$$\int_0^\infty \sigma(\omega)\, d\omega = \omega_p^2. \tag{7.2}$$

Given the constraint (3.5) the allowed density fluctuations determining ω_p^2 are only between the one-hole and the two-hole states ϕ_i. From Eq. (4.26) the density of the two-hole states is x. Therefore $\omega_p^2 \sim x(1-x)$. A proportionality of Eq. (7.2) to x for $x \lesssim 0.2$ has been noted experimentally.[59]

In regime III, where the integrated fluctuation spectra is $\sim\omega/G$, a crossover from $\rho(T)\sim T$ to T^2/G and a corresponding change in $\sigma(\omega)$ is predicted below $T\sim G$.

2. Thermal conductivity

The graphs of Fig. 13 with energy current external vertices give the thermal conductivity $\kappa(T)$. The usual kinetic theory expression follows:

$$\kappa(T) \approx \tfrac{1}{3} C_v(T) \langle v_F^2 \rangle \tau_{\mathrm{th}}(T), \tag{7.3}$$

with $\tau_{\mathrm{th}}^{-1}(T) = \lambda_{\mathrm{th}} T$ and $C_v(T) \approx T \ln(\omega_c/T)$. λ_{th} departs from λ_{mom} by numerical factors due to the different angular averages in momentum and thermal transport. The Wiedemann Franz ratio $\kappa(T)/T\sigma(T)$ is expected to be $\sim(\lambda_{\mathrm{th}}/\lambda_{\mathrm{mom}})\ln(\omega_c/T)$.

3. Raman scattering intensity

As has been discussed before the Raman intensity in a lattice has a part proportional to the current-current correlation function and hence

$$S_R(\omega,T) \sim [n(\omega/T)+1]\omega\sigma(\omega,T). \tag{7.4}$$

So a Raman intensity independent of frequency and temperature near the ideal composition is expected as observed. Crossover to a behavior linear in ω at low ω in regimes II and III is predicted and has been observed in regime II with a crossover to regime I under pressure. In principle, such $S_R(\omega,T)$ is expected in all polarizations, and the relative intensity may in general be quite different.

The collective fluctuations (5.10) also couple directly in the Raman experiment. But since $\mathrm{Im}D(0,\omega)\sim\omega\sigma(\omega,T)$, this also gives the behavior of Eq. (7.4).

C. NMR and inelastic magnetic neutron scattering

The application of the theory to the NMR properties has been also described elsewhere;[61] only the principal points are summarized here. The current fluctuations (5.10) generate an orbital magnetic field which vanishes at $q=0$ both at the copper site and the oxygen site as may be seen from Fig. 10. At finite q, an orbital magnetic field proportional to q is generated at the copper sites but not at the oxygen sites. This is because around the fourfold-coordinated Cu site a circulating current due to the electrons can be constructed to O (q), but not at the twofold-coordinated oxygen site. This gives rise to an anomalous orbital contribution to the magnetic correlation functions at the Cu sites:

$$\mathrm{Im}\chi_{\mathrm{orb}}(q,\omega) \approx \mu_B^2 (qa)^2 \left(\frac{a_0}{a}\right)^6 \mathrm{Im}D(q,\omega), \tag{7.5}$$

where a_0 is the radius of the Cu d orbital. The nuclear relaxation rate calculated using Eq. (7.5) has the correct temperature dependence to fit the observations on Cu.[57] Oxygen nuclear relaxation rate follows the Koringa law.

One of the most important aspects of the experimental results[24,29] is that the oxygen relaxation rate divided by the oxygen Knight shift does not vary either with x or from compound to compound within experimental uncertainty. Given this fact and the fact that antiferromagnetic fluctuations, to the extent they are seen, change the position of their peak and their width with x, it is impossible to take seriously proposals which rely on the cancellation of such fluctuations at oxygen sites to account for the observations. A more robust symmetry is called for. In the picture presented here lattice symmetry never allows $\chi_{\mathrm{orb}}(q,\omega)$ at oxygen sites.

The predicted $\chi_{\mathrm{orb}}(q,\omega)$, Eq. (7.5), can be measured by inelastic neutron scattering. Perhaps inelastic x-ray scattering can help distinguish the orbital magnetic fluctuations from spin fluctuations. Equation (7.5) predicts an unusually smooth q dependence and scattering up to the high-energy cutoff at any q. The measured q-integrated magnetic fluctuation spectrum in $La_{1.85}Sr_{0.15}CuO_4$ is consistent[21] with Eq. (7.5). Further tests are suggested especially in compounds where nesting features of the band structure do not introduce sharp q-dependent features at low energies. A direct test of the theory would be inelastic neutron scattering experiments in several Brillouin zones and transformation back to real space to deduce separately the magnetic fluctuations on oxygen and on Cu. Only a Fermi-liquid contribution $\sim N(0)\omega/qv_F$ for $\omega \lesssim qv_F$ and 0 beyond should be seen on oxygen, which in appropriate range is negligible compared to Eq. (7.5), which should be seen only on Cu.

VIII. EFFECTS OF IMPURITIES

The problem of disorder in a non-Fermi liquid is complicated (and interesting). Only a preliminary treatment of some ideas is presented here to clarify aspects of the phase diagram of copper oxides in the underdoped regime and the fate of the transition to the circulating current phase in the presence of disorder.

First consider the effect of disorder in the transition from phase I to phase II, the circulating current phase. The Harris criteria[62] may be used in the classical regime of the transition

to determine if quenched disorder, which varies the *local* transition temperature $T_c(r)$ is *relevant*. This is derived by equating the free-energy contribution due to fluctuation in $T_c(r)$ in a correlation volume to the pure fluctuation energy in the same volume. If

$$d\nu - 2 < 0, \tag{8.1}$$

disorder is relevant. Here ν is defined in terms of the correlation length as $\xi \sim (T - T_c)^{-\nu}$ for a fixed x. In the Gaussian fluctuation regime, $\nu = 1/2$ while in the critical fluctuation regime for the $d=2$ Ising model $\nu = 1$, and so disorder is relevant in the former and marginally irrelevant in the latter. This is expected to be true at asymptotically high temperatures far away from $x = x_c(0)$ in the phase diagram, Fig. 12.

Now consider the transition at $T=0$ as a function of $[x - x_c(0)]$. At $T=0$ only zero frequency fluctuations come to play. So the dynamical critical exponent z_d cannot affect the relevance of disorder. The Harris criteria may be expected to therefore to be valid, but we should define ν through ($\nu \equiv \nu_0$), $\xi \sim [x - x_c(0)]^{-\nu_0}$. Using Eq. (5.10) and noting that at $\omega = 0$, $T = 0$, $\ln|x - x_c(0)|$ scales as q^2, $\nu_0 = 0$. The Harris criteria then suggests that disorder is strongly relevant. Not much definite appears to be known about the physical state when this is the case. The best guess is that the phase transition turns into a crossover and that a glassy low-temperature phase results with random local orientations of the order parameter. This is quite reasonable when correlation lengths are short ($\nu_0 = 0$); there is local ordering around each defect with no correlations building up between regions around different defects.

To summarize the above, the correlation length exponent changes from 0 to its classical Ising value at asymptotically high temperatures and large $x_c(0) - x$. Correspondingly one expects only a crossover in the x-T plane to a glassy circulating current phase.

The problem is even more interesting because the single-particle excitations begin to acquire more singular self-energy than Eq. (1.1) or (6.4) due to defects. It was conjectured[8] that a non-Fermi liquid is an insulator for arbitrarily small disorder (resistivity $\to \infty$ as $T \to 0$) if superconductivity does not intervene at a higher temperature. In recent calculations this conjecture has been supported by some systematic calculations.[63] The result of these calculations is that the impurity contribution to the resistivity in a marginal Fermi liquid is proportional to $\ln T$ below a crossover temperature

$$T_x \approx (\omega_c/\pi)\exp(-\lambda^{-1}\sqrt{k_F \ell_0}). \tag{8.2}$$

Here ℓ_0 is the mean free path due to impurities calculated in the Born approximation. Below such an energy scale the density of states at the chemical potential also tends to zero, as $(\ln\omega)^{-1}$.

The observed low-temperature resistivity in dirty samples or in samples in which superconductivity is suppressed by a large magnetic field (as well as the temperature dependence of the anisotropy in the resistivity) is consistent with these calculations.[64] These calculations rely on using the marginal self-energy to calculate the impurity scattering vertex through a Ward identity. The experiment gives a $\ln T$ resistivity in a wide range of doping in underdoped samples, where in the pure limit the fluctuations have a gap and a marginal self-energy is not expected. One possible way this can happen is if the fluctuations acquire a finite low-energy spectral weight due to disorder. This would be consistent with excitations in the glassy state conjectured above.

IX. SUPERCONDUCTIVE INSTABILITY

It is only natural that the fluctuations responsible for the anomalous normal state also lead to the instability to superconductivity. We again look to the low-energy Hamiltonian, Eq. (6.1), to deduce the effective interaction in the particle-particle channel. As usual, this gives for total momentum of the pair equal to zero:

$$H_{\rm pair} = \sum_{k,k'} g(k,k')g^*(-k,-k')D(k-k',\omega)$$
$$\alpha^\dagger_{-k\sigma'''}\alpha^\dagger_{-k'\sigma''}\alpha_{-k\sigma'}\alpha_{k\sigma}. \tag{9.1}$$

Equation (9.1) is now used to deduce the symmetry channel with the largest pairing interaction. The procedure followed is the generalization to more than one atom per unit cell case of that in Ref. 65, where it was shown that antiferromagnetic fluctuations promote even-parity spin-singlet pairing which has ''d-wave'' symmetry in metals with appropriate band structures. The situation here is much more complicated; a preliminary analysis is given below. The propagator $D(q,\omega)$ is to a very good approximation independent of momentum for frequencies ω of importance for pairing which are always higher than T. So D can be regarded as a constant, D_0 with an upper frequency cutoff ω_c. The effective pairing Kernel is then

$$\sim \begin{pmatrix} 3 \\ -1 \end{pmatrix} g_0^2 D_0 |\mathcal{F}_y(k) + \mathcal{F}_y(k')|^2 \sin^2\left(\frac{\lambda_k - \lambda_{k'}}{2}\right), \tag{9.2}$$

where uppercase corresponds to spin-singlet (even parity) and lowercase to spin-triplet (odd parity) pairing. We wish to express this as a sum over products of functions of k and k' which have the symmetry of the lattice and which are mutually orthogonal. Sticking to the lowest lattice harmonics, we look for coefficients in the expansion

$$(3)[J_S + J_A A(k)A(k') + J_D D(k)D(k') + \cdots], \tag{9.3}$$

$$(-1)[J_t(T_{kx}T_{k'x} + T_{ky}T_{k'y}) + \cdots], \tag{9.4}$$

where J_S is the coefficient for the simple s-wave pairing, J_A for pairing of ''extended s-wave form,'' i.e.,

$$A(k) = \cos k_x a + \cos k_y a, \tag{9.5}$$

J_D for pairing of ''d-wave form,'' i.e.,

$$D(k) = \cos k_x a - \cos k_y a, \tag{9.6}$$

and J_t for the odd-parity form $\sin k_x a$ or $\sin k_y a$. The ellipses in Eqs. (9.3) and (9.4) refer to higher lattice harmonics, i.e., periodic functions of $2k_x a$, $2k_y a$, and so on, which we ignore and which are automatically mixed in to the gap function below T_c due to the nonlinearity in the gap equation. $\sin^2[(\lambda_k - \lambda_{k'})/2]$ in Eq. (9.2) is a very complicated function, but it has two properties which help write down the leading

dependence on k,k' consistent with lattice symmetry. It is zero for $k=k'$ and peaks when the difference momenta is maximum possible, i.e., at $(k_x=k_x'=\pi/a,\ k_y-k_y'=\pi/a)$. The lowest lattice harmonic satisfying these conditions is

$$1-\tfrac{1}{2}[\cos(k_x-k_x')a+\cos(k_y-k_y')a]. \tag{9.7}$$

In $|\mathcal{F}_y(k)+\mathcal{F}_y(k')|^2$, the only part I keep is a constant; the others give harmonics. One then gets the relative magnitudes in units of $g_0^2 D_0 \approx \lambda N^{-1}(0)$:

$$s\text{-wave pairing:}\quad 3J_S=3;$$

$$D\text{-wave pairing:}\quad 3J_D=-3/2;$$

$$\text{extend } s\text{-wave pairing:}\quad 3J_A=-3/2;$$

$$\text{triplet pairing:}\quad J_t=+1.$$

This immediately implies that simple s-wave pairing and triplet pairing Kernels are repulsive. In the present case simple s-wave pairing is disallowed simply from the fact that the effective interaction vanishes at long wavelength, and the triplet is disallowed because the fluctuations conserve spin. The kernels for D-wave and extended s-wave pairing are attractive and of equal magnitude. The situation is thus identical to the case of antiferromagnetic fluctuations with fluctuations peaking at $(k_x a=\pi,\ k_y a=\pi)$.

The T_c is determined, as usual, from the linear gap equation projected to the lattice harmonics. T_c^D for D-wave pairing is in general different than T_c^A, depending purely on the band structure, and the chemical potential, exactly as for the case of antiferromagnetic fluctuations. For that case and with Cu-O band structure on a square lattice d-wave pairing is formed to be favored in explicit calculations. The large density of states due to the proximity to van Hove singularities in the (π,π) direction favors d-wave pairing. The same is therefore expected in the present case. Just as for antiferromagnetic fluctuations, variations in the band structure near the Fermi surface give superconducting states of different symmetries for the same interaction vertex.

The upper cutoff ω_c of $D(q,\omega)$ is of $O(E_F)$; from a fit to normal-state transport experiments, the coupling $\lambda \approx 0.5$. As for normal-state transport, vertex corrections are unimportant for calculations of T_c, etc. So a consistent theory can be built.

It is worth noting that a signature of the glue for superconductivity is provided by the tunneling conductance. Under appropriate experimental conditions, as discussed in Sec. VII A and Ref. 14, $dG(V)/dV$ (above the superconducting gap) is proportional to the density of state of the glue for superconductivity weighted by the q dependence of the coupling constant: the famous ''$\alpha^2(\omega)F(\omega)$.''[57] The present theory predicts this to be a constant (with small corrections) up to the cutoff ω_c. This is indeed observed but only in some geometries for reasons discussed in Ref. 14. Further systematic studies are called for. Optical conductivity in the superconducting phase for frequencies larger than twice the gap also can be used to deduce the glue for superconductivity.[66] The existing data are again consistent with the form (5.10).

The results of Ref. 65 show that any bosonic fluctuations such that the pairing interaction is miminal for $q=0$ and maximum for $q=(\pi,\pi)$ produce d-wave pairing. To distinguish between mechanisms requires the experiments discussed above.

X. CONCLUDING REMARKS, FURTHER THEORY, AND FURTHER EXPERIMENTS

This investigation has been based on two basic assumptions: (i) Breakdown of Landau theory in more than one dimension requires scale-invariant low-energy fluctuations. (ii) The solid-state chemistry of copper oxide is special and responsible for its special physical properties. Accordingly, I have formulated the copper-oxide model of Sec. II and tried to investigate its properties in a systematic manner to find unusual singular low-energy fluctuations. The model does have an antiferromagnetic instability at small doping. It probably has other finite-q instabilities at larger x for a range of parameters, especially if there is a nesting of the Fermi surface. Given the experimental data, I do not regard the singular fluctuations near such instabilities as a solution to the fundamental problems stated in Sec. I. I have found a $q=0$ transition to an unusual circulating current phase on a line the x-T plane in the general model in the pure limit terminating at a quantum critical point at $x=x_c$, $T=0$. The model has unusual low-energy fluctuations in which the logarithm of the frequency scales with the momentum, so that the fluctuations are essentially local in space. Such local fluctuations are essential to understand the peculiar normal-state transport anomalies in which the momentum scattering rate, energy scattering rate, and the single-particle scattering rate are all proportional to T. They have the right energy scale to give a ''continuous behavior'' in optical and Raman conductivities from zero frequency to energies of $O(1\text{ eV})$. The current fluctuations also produce local orbital magnetic field fluctuations which have the symmetry and temperature dependence to account for the extraordinary NMR relaxation rates on Cu and O nuclei. The fluctuations also couple to fermions to give a superconducting instability with d-wave symmetry favored. Disorder appears to convert the transition line to the circulating current phase to a crossover line due to the quasilocal nature of the fluctuations.

There exist several incomplete aspects of the theory presented here. While it has been shown conclusively that the circulating current instability does indeed occur in the model, the phase diagram in the T-x plane has not been determined. This requires an explicit numerical solution of the mean-field equations (4.27)–(4.29) with an assumed set of reasonable parameters. I have relied on Refs. 50–52 and general analyticity conditions for fluctuations near an instability to present a heuristic derviation of the form of the fluctuation spectrum, Eqs. (4.35) and (4.36). A better calculation is desirable. A detailed treatment of the different regimes of fluctuations and the effect of disorder is needed. A complete examination of the superconductive instability $T_c(x)$ is possible and should be done.

What are the principal experiments on which this paper has been silent? First is the question of the very interesting magnetotransport anomalies.[25,26] I have indicated in Sec. I that the experimental results do not appear to show that they

have asymptotic low-energy and low-temperature singularities. But even so, the peculiar subleading behavior ought to be calculated. It is true that circulating current fluctuations lead to chiral scattering in a perpendicular magnetic field. As noted in Ref. 28, the temperature dependence of such chiral scattering is reflected in the magnetotransport anomalies. But so far I have not succeeded in formulating their effect consistently. Second, very interesting changes in angle resolved photoemission spectra[67] have been observed in going from region 1 to region 4 of the phase diagram of Fig. 1. It would be very natural to try to associate these with the transition or crossover to the circulating current phase. The observed changes in the spectra are most pronounced where the Fermi surface of the ideally doped samples crosses the $(\pi,0)$-(π,π) direction and least pronounced where the Fermi surface crosses the (0,0)-$(\pi,0)$ direction; i.e., the changes have x^2-y^2 symmetry. As discussed in Sec. IV E the changes in the one-particle spectra in the circulating current phase also do have x^2-y^2 symmetry. This is quite intriguing but a calculation of the one-particle spectral function in the circulating current phase is necessary to draw any conclusions. Third, there are aspects of NMR experiments, especially the anisotropy in the relaxation rate, which are not explained in Ref. 61. Understanding anisotropy effects in NMR requires a theory of the coupling of fluctuation between different planes.

Are there experiments left to do after the $O(5\times10^4)$ already published to test the conclusions of this paper? The answer is yes, but most of them are difficult experiments.

The most direct and convincing test of the theory would be the observation of the circulating current phase in the underdoped samples and its evolution as a function of temperature. As discussed earlier, long-range order is unlikely but correlation lengths should be large in very pure samples. The current patern in Fig. 6 can be observed by Bragg scattering of polarized neutrons or polarized x rays. I estimate that with polarized neutrons the spin-flip cross section in the circulating current phase at the (1,1) Bragg peak is $O(10^{-3})$ the nuclear cross section.

Another test would be evidence for local magnetic fields in regions 4 and 2 which are estimated to be $O(50$ G). As shown in Fig. 6, the local field is interstitial; there is no magnetic field either on Cu or O lattice sites. Muon spin resonance would be a way to look for interstitial fields if muons were to sit at the interstitial sites indicated in Fig. 6.

As noted, the spectrum of current fluctuations at $q=0$ as a function of ω, T, and x is directly observable in Raman scattering. A direct test of the theory would be evidence for the fluctuation spectra of Eq. (5.10) at large q and the difference in its projection on to the Cu and O sites obtainable by scattering in several Brillouin zones mentioned above. In the section on NMR and inelastic neutron scattering, I mentioned that existing neutron scattering in $La_{1.85}Sr_{.15}CuO_4$ is consistent with the magnetic fluctuations[21] derived from Eq. (5.10). More detailed tests, especially with scattering over a large range in momentum and frequency in $YBa_2Cu_3O_{6.9}$ which shows no nesting related peaks in q space, are suggested.

In very pure samples of $YBa_2Cu_3O_{6.7}$ and (248), which at stoichiometry behaves as an underdoped material, the sliver region 4 between regions 1 and 2 in Fig. 1 where the resistivity falls below the extrapolation from high temperatures clearly appears. The crossover to the circulating current phase in such samples should not be two broad. One should look for signatures of this in thermodynamic experiments, specific heat, and magnetic susceptibility which should show a bump near the crossover and a significant decrease below. Such samples at low temperatures would be particularly suitable to look for direct evidence discussed above the circulating current phase.

The conjecture about magnetotransport[28] and the behavior of the critical fluctuations in a magnetic field can be tested by a Raman scattering experiment in a magnetic field. The polarized part of the spectra proportional to the magnetic field should acquire singular low-energy, low-temperature form.

Some of the other tests of the theory have already been mentioned. These include (i) improved angle-resolved photoemission experiments to verify Eq. (6.4) and its modifications due to impurities deduced in Ref. 63, (ii) measurement of the electronic specific heat in low-T_c copper oxides (for example, the single-layer Bi compound with $T_c\approx10$ K near ideal composition) to see the $T\ln T$ contribution to the electronic specific heat, (iii) controlled single-particle tunneling experiments to see the spectrum of the ''glue'' for superconductivity. It should be mentioned that optical conductivity and Raman scattering experiments for $\omega>2\Delta$ can also be used to deduce the spectrum of the ''glue,'' and very importantly, (iv) inelastic neutron scattering in two or more Brillouin zones to deduce the projection of $\chi(q,\omega)$ separately on the Cu and O atoms.

ACKNOWLEDGMENTS

I have benefited through comments and discussions on this work by G. Kotliar, P. Majumdar, A. Ruckenstein, A. Sengupta, and Q. Si. Appendix B is primarily the work of Q. Si. He also helped improve Sec. III considerably. Over the years I have benefited through collaborations and discussions on the copper-oxide problem with E. Abrahams, G. Aeppli, B. Batlogg, E. I. Blount, T. Giamarchi, Y. Kuroda, P. B. Littlewood, O. Narikiyo, P. Nozieres, K. Miyake, S. Schmitt-Rink, C. Sire, A. Sudbo, and R. E. Walstedt. Discussions with B. I. Halperin, D. Huse, and S. Sachdev on aspects of critical phenomena relevant to this work are also gratefully acknowledged.

APPENDIX A: ONE-ELECTRON BAND STRUCTURE AND EIGENVECTORS

The band structure and the eigenvectors for H_0 of Eq. (2.2) for $t_{pp}/t_{pd}\ll1$ are given here. For $t_{pd}=0$, the bonding b and the antibonding a bands have dispersions

$$\epsilon^0_{a,b}(\mathbf{k})=\pm[(\Delta_0/2)^2+4t_{pd}^2s_{xy}^2(k)]^{1/2}, \tag{A1}$$

where $s_{xy}^2(\mathbf{k})=\sin^2(k_ya/2)$ and the nonbonding band n is nondispersive with energy $-\Delta_0/2$. The eigenvectors may be specified by the band annihilation operators in terms of these in the orbitals $d^\dagger_{k\sigma}$, $p^\dagger_{xk\sigma}$, $p^\dagger_{yk\sigma}$ as in Eq. (2.5).

The coefficients in (2.5a) and (2.5b) for $t_{pp}=0$ (specified by a superscript 0) are

$$u^0_{ad}(k)=[\Delta/2+\epsilon^0_a(k)]/N_a(k), \tag{A2}$$

$$u^0_{ax,y}(k)=2it_{pd}/N_a(k),$$

$$u^0_{bd}(k)=[\Delta/2+\epsilon^0_b(k)]/N_b(k),$$

$$u^0_{bx,y}(k)=-2it_{pd}/N_b(k),$$

where $N_{a,b}(k)=\{[\Delta/2+\epsilon^0_{a,b}(k)]^2+4t^2_{pd}s^2_{x,y}(k)\}^{1/2}$. The nonbonding orbital has an energy $-\Delta/2$ and is annihilated by

$$i[\sin(k_ya/2)p_{xk}-\sin(k_xa/2)p_yk]/s_{xy}(k). \tag{A3}$$

The changes in the coefficients in Eqs. (2.5a) and (2.5b) are calculated to first order in t_{pp} using as a perturbation the O-O hopping Hamiltonian

$$H_1=4t_{pp}\sum_{k,\sigma}\sin\left(\frac{k_xa}{2}\right)\sin\left(\frac{k_ya}{2}\right)p^\dagger_{xk\sigma}p^\dagger_{yk\sigma}+\text{H.c.}, \tag{A4}$$

$$u_{ad}(k)=u^0_{ad}(k)+f_{ab}(k)u^0_{bd}(k),$$

$$u_{ax}(k)=s_x[u^0_{ax}(k)-f_{ab}u^0_{by}(k)]+f_{ac}u^0_{ay}s_y, \tag{A5}$$

$$u_{ay}(k)=s_y[u^0_{ay}(k)-f_{ab}u^0_{ax}(k)]-f_{ac}u^0_{ay}s_x.$$

For the coefficients in Eq. (2.5b) replace $a\leftrightarrow b$ in Eq. (A4). In Eq. (A4) ,

$$f_{ab}(k)=\frac{4t_{pp}}{(\epsilon^0_{bk}-\epsilon^0_{ak})}\frac{\sin^2(k_xa/2)\sin^2(k_ya/2)}{s^2_{xy}(k)}u^0_{ax}(k)\;\;u^0_{by}(k)$$
$$=f_{ba}(k),$$

$$f_{ac}(k)=\frac{4t_{pp}}{(\Delta_0/2-\epsilon^0_{ak})}\frac{\sin^2(k_xa/2)-\sin^2(k_ya/2)}{s^2_{xy}(k)}\sin\frac{k_xa}{2}\sin\frac{k_ya}{2}$$
$$=-f_{bc}(k). \tag{A6}$$

APPENDIX B: EXCHANGE HAMILTONIAN IN τ SPACE

Here, the exchange Hamiltonian (3.18) is derived from the strong-coupling limit where the high-energy states described in Sec. III A are eliminated by a canonical transformation.

As usual in such a procedure, we write the Hamiltonian as

$$H=H_{\text{low}}+H_{\text{high}}+H_{\text{mix}}, \tag{B1}$$

where H_{low} contains the low-energy states we wish to keep, i.e., states $d^\dagger_{1i\sigma}|0\rangle$, $d^\dagger_{2i\sigma}|0\rangle$. H_{high} are the states we wish to discard and H_{mix} connects states in H_{low} and H_{high}. We introduce a canonical transformation

$$\tilde{H}=e^{iS}He^{-iS}, \tag{B2}$$

such that, to linear order in H_{mix}, matrix elements connecting states of H_{low} and H_{high} vanish. This requires that S be determined by

$$H_{\text{mix}}+i[S,H_{\text{low}}+H_{\text{high}}]=0. \tag{B3}$$

The transformed Hamiltonian, to second order in H_{mix}, is

$$\tilde{H}=H_0+i[S,H_{\text{mix}}]. \tag{B4}$$

H_0 is the kinetic energy (3.4) and (3.16). We give the results for elements of $[S,H_{\text{mix}}]$ in the approximation that all the *neglected states* specified in Sec. III A except the zero-hole state (with energy 0) are assumed to be infinitely high compared to the low-energy states: the two one-hole states at energy $\mp\Delta-\mu$ and the two-hole state at energy $E_\phi=V-2\mu$. (No essential difference arises in the more general and messy situation.) Accordingly, we write the kinetic energy in terms of operators $d_{1i\sigma}$ and $d_{2i\sigma}$ using Eqs. (3.6), (3.7) and the first term of Eq. (3.17):

$$d^\dagger_{i\sigma}=\frac{1}{\sqrt{2}}\text{sgn}\sigma\phi^\dagger_i d_{2i-\sigma}+d^\dagger_{1i\sigma}\phi_{0i}, \tag{B5}$$

$$D^\dagger_{i\sigma}=\frac{1}{\sqrt{2}}\text{sgn}\sigma\phi^\dagger_i d_{1i-\sigma}+d^\dagger_{2i\sigma}\phi_i.$$

The bare kinetic energy or H_{mix}, Eq. (3.4), is

$$H_{\text{mix}}=\sum_{i<j,\sigma}t^{dD}_{ij}d^\dagger_{i\sigma}D_{j\sigma}+t^{dd}_{ij}d^\dagger_{i\sigma}d_{j\sigma}+t^{DD}_{ij}D^\dagger_{i\sigma}D_{j\sigma}+\text{H.c.} \tag{B6}$$

Inserting Eq. (A5) into Eq. (A6), we solve for S in Eq. (A3) by taking matrix elements between the states of $H_{\text{low}}+H_{\text{high}}$ of known energy. S is then inserted into Eq. (A4). The second term gives the exchange Hamiltonian of the form (3.19). The part in spin $\boldsymbol{\sigma}$ space is isotropic because of rotational invariance in $\boldsymbol{\sigma}$ space. The part in (d_1-d_2) space is specified as

$$(\tau^i_y\;\tau^i_x\;\tau^i_z)M\begin{pmatrix}\tau^i_y\\ \tau^i_x\\ \tau^i_z\end{pmatrix}. \tag{B7}$$

M has the form

$$\begin{pmatrix}M_{yy}&0&0\\0&M_{xx}&M_{xz}\\0&M_{zx}&M_{zz}\end{pmatrix}, \tag{B8}$$

which we already discussed is the most general form allowable.

We find that with $E_\phi\pm2\Delta\equiv E_\pm$ and $E^{-1}_+ + E^{-1}_-\equiv\overline{E^{-1}}$:

$$M^{ij}_{yy}=-2\;t^{ij}_{dd}t^{ji}_{DD}/E_\phi+(t^{ij}_{dD})^2/\overline{E},$$

$$M^{ij}_{xx}=-2t^{ij}_{dd}t^{ji}_{DD}/E_\phi-(t^{ij}_{dD})^2/\overline{E},$$

$$M^{ij}_{zz}=(t^{ij2}_{dd}+t^{ij2}_{DD})/E_\phi-(t^{ij}_{dD})^2/\overline{E}, \tag{B9}$$

$$M^{ij}_{zx}=M^{ij}_{xz}=\frac{1}{2}t^{ij}_{dD}(t^{ji}_{dd}+t^{ji}_{DD})\left(\frac{1}{E_+}+\frac{1}{E_-}\right).$$

A rotation, Eqs. (3.32) and (3.33) about τ_y, which diagonalizes the kinetic energy to a-b space of Sec. IV, is used to get the Hamiltonian which on Fourier transforming gives Eq. (4.2). For the special case $\Delta=0$, the rotation is by an angle $\pi/4$. In that case and if $t_{dd}=t_{DD}=0$,

$$\mathcal{J}_{\perp}=t_{dD}^2/E_{\phi}, \quad \mathcal{J}_{zz}=0,$$
$$(\mathcal{J}_{xx}-\mathcal{J}_{yy})=-t_{dD}^2/E_{\phi}, \tag{B10}$$
$$\mathcal{J}_{zx}=\tfrac{1}{2}t_{dD}^2/E_{\phi}.$$

Then for $\langle\tau_z\rangle=1$, $A+2B=0$. For the more general case, a condition on Δ or x can always be found, so that the condition for a QCP derived in Sec. IV; i.e., $\pm A+2B+4C=0$ is fulfilled.

[1] (a) The most complete references to the experimental results are the proceedings of the last two triannual international conferences on materials and mechanisms of superconductivity: edited by M. Tachiki, Y. Muto and Y. Syono [Physica C **185-189** (1991)]; edited by P. Wyder [Physica C **235-240** (1994)]; (b) A source of excellent review articles is the series *Physical Properties of High Temperature Superconductors*, edited by D. M. Ginsburg [World Scientific, Singapore, Vol I (1989), Vol II (1990), Vol. III (1992), Vol. IV (1994)].

[2] For a particularly clear exposition of Landau's phenomenological theory, see Chap. I of D. Pines and P. Nozières, *Quantum Liquids* (Benjamin, New York, 1964), Vol. I; for a microscopic derivation, see Chap. IV of A. A. Abrikosov, L. P. Gorkov, and I. E. Dzyaloshinksii, *Methods of Quantum Field Theory in Statistical Physics* (Prentice Hall, Englewood Cliffs, NJ, 1963); P. Nozières, *Interacting Fermi Systems* (Benjamin, New York, 1964).

[3] S. Martin *et al.*, Phys. Rev. B **41**, 846 (1990).

[4] J. W. Loram *et al.*, Physica C **235**, 134 (1994); J. Supercond. **7**, 243 (1994).

[5] R. Shankar, Rev. Mod. Phys. **66**, 129 (1994); C. Castellani, C. DiCastro, and W. Metzner, Phys. Rev. Lett. **72**, 316 (1994); A. Houghton and J. B. Marston, Phys. Rev. B **48**, 7790 (1993), A. H. Castro Neto and E. Fradkin, Phys. Rev. Lett. **72**, 1393 (1994).

[6] For an alternative point of view that the physics in more than one dimension is similar to one dimension, see P. W. Anderson, Phys. Rev. Lett. **64**, 1839 (190); **65**, 2306 (1992); P. W. Anderson and D. Khevschenko (unpublished).

[7] H. Takagi *et al.*, Phys. Rev. Lett. **69**, 2975 (1992).

[8] G. Kotliar *et al.*, Europhys. Lett. **15**, 655 (1991).

[9] Y. Fukuzumi *et al.*, Phys. Rev. Lett. **76**, 684 (1996).

[10] B. Bucher *et al.*, Physica C **157**, 478 (1989).

[11] T. Zhou, K. Syassen, M. Cardona, J. Karpinski, and E. Kaldis, Solid State Commun. **99**, 669 (1996).

[12] (a) C. M. Varma, P. B. Littlewood, S. Schmitt-Rink, E. Abrahams, and A. E. Ruckenstein, Phys. Rev. Lett. **63**, 1996 (1989); C. M. Varma, Int. J. Mod. Phys. **3**, 2083 (1989); (b) P. B. Littlewood and C. M. Varma, J. Appl. Phys. **69**, 4979 (1991).

[13] J. Hertz, Phys. Rev. B **14**, 1165 (1976); M. T. Beal-Monod and K. Maki, Phys. Rev. Lett. **34**, 1461 (1975); A. V. Chubukov, S. Sachdev, and J. Ye, Phys. Rev. B **49**, 11 919 (1994); S. Sachdev, in *Proceedings of the 19th IUPAP Conference on Statistical Physics*, Xiamen, China, edited by B.-L. Hao (World Scientific, Singapore, 1996); A. J. Millis, Phys. Rev. B **48**, 7183 (1993).

[14] P. B. Littlewood and C. M. Varma, Phys. Rev. B **45**, 12 636 (1992).

[15] C. G. Olson *et al.*, Science **245**, 731 (1989).

[16] T. Timusk and D. B. Tanner, in Vol. I (1989) and Vol. III (1992) of Ref. 1(b).

[17] Some review articles are C. Thomsen, in *Light Scattering in Solids VI*, edited by M. Cardona (Springer-Verlag, New York, 1991); G. Guntherodt, *ibid.*; D. Einzel and R. Hackl, J. Raman Spectrosc., **27** (1996).

[18] C. Uher, in Vol. III, pp. 159–284 of Ref. 1(b).

[19] For an alternative point of view, see, for example, T. Moriya, Y. Takahashi, and K. Ueda, J. Phys. Soc. Jpn. **59**, 2905 (1990); P. Monthoux and D. Pines, Phys. Rev. B **47**, 6069 (1993).

[20] J. M. Tranquada *et al.*, Phys. Rev. B **46**, 5561 (1992); J. Rossat-Mignod *et al.*, Physica B **192**, 109 (1993); L. P. Regnault *et al.*, Physica C **235**, 59 (1994); B. Keimer *et al.* (unpublished).

[21] T. E. Mason *et al.*, Phys. Rev. Lett. **71**, 919 (1993); S. M. Hayden *et al.*, *ibid.* **76**, 1344 (1996).

[22] For an alternative point of view see V. J. Emery and S. A. Kivelson, Physica C **209**, 597 (1993), and Ref. 23.

[23] C. Castellani, C. DiCastro, and M. Grilli, Phys. Rev. Lett. **75**, 4650 (1995).

[24] An excellent review article is C. H. Pennington and C. P. Slichter, in Vol. III of Ref. 1(b).

[25] (a) T. R. Chien, Z. Z. Wang, and N. P. Ong, Phys. Rev. Lett. **67**, 2088 (1991); J. M. Harris, Y. F. Yan, and N. P. Ong, Phys. Rev. B **46**, 14 293 (1992); (b) H. Y. Hwang *et al.*, Phys. Rev. Lett. **72**, 2636 (1994).

[26] J. M. Harris *et al.*, Phys. Rev. Lett. **75**, 1391 (1995).

[27] W. E. Pickett *et al.*, Rev. Mod. Phys. **61**, 433 (1989).

[28] G. Kotliar, A. Sengupta, and C. M. Varma, Phys. Rev. B **53**, 3573 (1996).

[29] C. Berthier *et al.*, Phys. Scr. **T49**, 131 (1993).

[30] Y. Kuroda and C. M. Varma, Phys. Rev. B **42**, 8619 (1990) and Ref. 12(b).

[31] M. Nuss *et al.*, Phys. Rev. Lett. **66**, 3305 (1991).

[32] See, for example, H. Ding *et al.*, Phys. Rev. Lett. **74**, 2784 (1995).

[33] D. J. Van Harlingen, Rev. Mod. Phys. **67**, 515 (1995); W. N. Hardy *et al.*, Phys. Rev. Lett **70**, 3999 (1993); C. C. Tsuei *et al.*, *ibid.* **73**, 593 (1994).

[34] A. G. Sun *et al.*, Phys. Rev. Lett. **72**, 2267 (1994).

[35] D. H. Wu *et al.*, Phys. Rev. Lett. **70**, 85 (1993).

[36] C. M. Varma, S. Schmitt-Rink, and E. Abrahams, Solid State Commun. **62**, 681 (1987); in *Novel Mechanisms of Superconductivity*, edited by V. Kresin and S. Wolf (Plenum, New York, 1987). A model with both Cu and O orbitals was proposed at the same time by V. Emery, Phys. Rev. Lett. **58**, 2794 (1987). But the ionic interactions played no role in that model.

[37] C. M. Varma, and T. Giamarchi, in *Strongly Interacting Fermions and High T_c Superconductivity*, Proceedings of the Les Houches Summer School of Theoretical Physics, Les Houches, 1991, edited by B. Doucot and J. Zinn-Justin (Elsevier, New York, 1995), Session LVI.

[38] J. Zaanen, G. A. Sawatzsky, and J. W Allen, Phys. Rev. Lett. **55**, 418 (1985).

[39] A. Sudbo *et al.*, Phys. Rev. Lett. **70**, 978 (1993); E. B. Stechel *et al.*, Phys. Rev. B **51**, 553 (1995); A. Sandvik and A. Sudbo, *ibid.* **54**, 3746 (1996).

[40] L. V. Keldysh and Yu V. Kopaev, Sov. Phys. Solid State **6**, 2219 (1965); J. des Cloizeaux, J. Phys. Chem. Solids **26**, 259 (1965); D. Jerome, T. M. Rice, and W. Kohn, Phys. Rev. **158**, 462 (1967).

[41] P. B. Littlewood, C. M. Varma, and E. Abrahams, Phys. Rev. Lett. **63**, 2602 (1989), P. B. Littlewood, Phys. Rev. B **42**, 10 075 (1990); Y. Bang *et al.*, *ibid.* **47**, 3323 (1993); S. Coppersmith and P. B. Littlewood, *ibid.* **42**, 3966 (1990); R. Putz *et al.*, *ibid.* **41**, 853 (1990).

[42] M. Grilli *et al.*, Phys. Rev. Lett. **67**, 259 (1991); Phys. Rev. B **47**, 3331 (1993); J. C. Hicks, A. E. Ruckenstein, and S. Schmitt-Rink, *ibid.* **45**, 8185 (1992).

[43] A preliminary and incomplete treatment is in C. M. Varma, Phys. Rev. Lett. **75**, 898 (1995). Specifically, the fluctuations are calculated only in the frozen Fermi-sea approximation, and the symmetry breaking of the circulating current phase is not specified.

[44] B. I. Halperin and T. M. Rice, in *Solid State Physics*, edited by F. Seitz, D. Turnbull, and H. Ehrenreich (Academic Press, New York, 1968), Vol. 21; H. J. Schulz, Europhys. Lett. **4**, 609 (1987); A. A. Nersesyan and G. E. Vachnadze, J. Low Temp. Phys. **77**, 293 (1989).

[45] I. Affleck and J. B. Marston, Phys. Rev. B **37**, 3774 (1988); G. Kotliar, *ibid.* **37**, 3664 (1988).

[46] Y. Ohta, T. Tohyama, and S. Maekawa, Phys. Rev. Lett. **66**, 1228 (1991).

[47] S. E. Barnes, J. Phys. F **6**, 1375 (1976); P. Coleman, Phys. Rev. B **29**, 3035 (1984); N. Read and D. M. Newns, J. Phys. C **16**, 3273 (1983). These methods have been used on the Cu-O model with nearest-neighbor interactions in Ref. 42.

[48] See, for instance, A. E. Ruckenstein, P. J. Hirschfeld, and J. Appel, Phys. Rev. B **36**, 857 (1987).

[49] G. Baskaran, Z. Zhou, and P. W. Anderson, Solid State Commun. **63**, 973 (1987).

[50] J. Gavoret, P. Nozieres, B. Roulet, and M. Combescot, J. Phys. (Paris) **30**, 987 (1969); A. E. Ruckenstein and S. Schmitt-Rink, Phys. Rev. B **35**, 7551 (1987). For a recent discussion of the effects of recoil, see P. Nozières, J. Phys. I **4**, 1275 (1994).

[51] G. D. Mahan, Phys. Rev. **163**, 612 (1967); P. Nozières and C. DeDominicis, *ibid.* **178**, 1097 (1969).

[52] M. Combescot and P. Nozieres, J. Phys. (Paris) **32**, 913 (1971).

[53] L. P. Gorkov and G. M. Eliashberg, Sov. Phys. JETP, **27**, 328 (1968).

[54] A. Ruckenstein and C. M. Varma, Physica C **185**, 134 (1991).

[55] T. Holstein, R. E. Norton, and P. Pincus, Phys. Rev. B **8**, 2647 (1973); M. Reizer, *ibid.* **39**, 1602 (1989).

[56] T. Hasegawa, M. Nantoh, and K. Kitazawa, Jpn. J. Appl. Phys. **30**, L276 (1991).

[57] J. R. Schrieffer, D. Scalapino, and J. W. Wilkins, Phys. Rev. **148**, 263 (1966); W. L. McMillan and J. M. Rowell, in *Superconductivity*, edited by R. D. Parks (Marcel Dekker, New York, 1969).

[58] E. Abrahams (private communication).

[59] See, for instance, J. Orenstein *et al.*, Phys. Rev. B **42**, 6342 (1990).

[60] Z. Schlesinger *et al.*, Phys. Rev. Lett. **65**, 801 (1990).

[61] C. M. Varma, Phys. Rev. Lett. **77**, 3431 (1996).

[62] A. B. Harris, J. Phys. C **7**, 1671 (1974).

[63] C. M. Varma (unpublished).

[64] Y. Ando *et al.*, Phys. Rev. Lett. **75**, 4662 (1995); (unpublished); S. Martin and C. M. Varma (unpublished); an analysis of results in S. Martin *et al.*, Phys. Rev. B **41**, 846 (1990).

[65] K. Miyake, S. Schmitt-Rink, and C. M. Varma, Phys. Rev. B **34**, 6554 (1986).

[66] See, for example, P. B. Allen, Phys. Rev. B **3**, 305 (1971).

[67] D. S. Marshall *et al.*, Phys. Rev. Lett. **76**, 4841 (1996); H. Ding *et al.*, Nature **382**, 51 (1996).